SAND77-0645
Unlimited Release

Computational and Experimental Methods for Enclosed Natural Convection

David W. Larson, David K. Gartling, Walter P. Schimmel, Jr.

Prepared by Sandia Laboratories, Albuquerque, New Mexico 87115
and Livermore, California 94550 for the United States Department
of Energy under Contract AT(29-1)-789

Printed October 1977

Sandia Laboratories

SF 2900 Q(7-73)

DISCLAIMER

Issued by Sandia Laboratories, operated for the United States Department of Energy by Sandia Corporation.

Printed in the United States of America

Available from
National Technical Information Service
U. S. Department of Commerce
5285 Port Royal Road
Springfield, VA 22161

Price: Printed Copy $4.50 ; Microfiche $3.00

SAND77-0645
Unlimited Release
Printed October 1977

COMPUTATIONAL AND EXPERIMENTAL METHODS FOR ENCLOSED NATURAL CONVECTION*

David W. Larson
Fluid Mechanics and Heat Transfer Div. II, 1262

David K. Gartling
Walter P. Schimmel, Jr.
Fluid Mechanics and Heat Transfer Div. I, 1261
Sandia Laboratories
Albuquerque, NM 87115

ABSTRACT

Two computational procedures and one optical experimental procedure for studying enclosed natural convection are described. The finite-difference and finite-element numerical methods are developed and several sample problems are solved. Results obtained from the two computational approaches are compared. A temperature-visualization scheme using laser holographic interferometry is described, and results from this experimental procedure are compared with results from both numerical methods.

*This work was partially supported by the LMFBR Spent Fuel Shipping Program which is funded by the Department of Energy Division of Reactor Development and Demonstration.

CONTENTS

FIGURES

CONTENTS (cont)

NOMENCLATURE

C_p	heat capacity
g	gravitational constant
k_{ij}	thermal conductivity tensor
n_j	outward unit normal
P	pressure
q_i	heat-flux vector
R	residual or error
s	coordinate along boundary
S	volumetric heat source
T	temperature
T_{ref}	reference temperature
u_i	velocity component
x_i	coordinate direction
β	coefficient of volume expansion
Γ	boundary
δ_{ij}	unit tensor
ρ	density
ν	kinematic viscosity
μ	viscosity
τ_{ij}	stress tensor
Φ, Ψ, Θ	shape function
ψ	stream function
ω	vorticity

COMPUTATIONAL AND EXPERIMENTAL METHODS FOR ENCLOSED NATURAL CONVECTION

Introduction

Recent years have seen considerable progress in efforts to develop computational procedures for solving the coupled conservation equations of motion (Navier-Stokes) and energy for an incompressible fluid. A large number of applied problems involving nonisothermal forced and/or free convection have stimulated the development of the numerical methods. Thermocline storage of solar-heated fluids, energy extraction from magma bodies, in-situ coal gasification, cooling of spent-fuel shipping casks, reactor core-meltdown accidents, radioactive waste disposal in the ocean, and numerous combustion problems are just a few of the many problems of current interest that need improved understanding.

A large measure of the needed insight for these systems could be provided by the numerical simulation of the appropriate fluid and thermal processes involved in a particular problem. Before engineering judgments can be confidently based on a numerical simulation, however, some form of validation of the numerical method must be obtained. The complexity of most coupled fluid/thermal problems precludes the possibility of obtaining closed-form analytic solutions for verification purposes. Therefore, quantitative experimental methods for investigating these flow fields are necessary to demonstrate the validity of the solutions to these complex but fundamental problems.

This report describes two computational procedures and one experimental procedure developed to investigate the problem of thermally driven enclosed natural convection. The numerical techniques include a finite-difference method (FDM) and a finite-element method (FEM). These methods are used to solve the coupled conservation equations resulting in determination of the temperature and velocity fields for the problem of interest.

The experimental technique is an optical procedure (laser holographic interferometry) that yields the temperature field of the thermal-convection problem.

Several sample problems are examined to demonstrate the capabilities and limitations of the numerical methods. Results obtained from the finite-difference and finite-element methods are compared. In addition, experimental results are compared with results from both computational procedures. The difficulties associated with accurate control of the boundary conditions during the experiments using early test sections prevent a detailed quantitative comparison of the numerical solutions with the experimental results. Nevertheless, the overall temperature field agreement obtained is remarkable.

Survey of Existing Methods

A large body of existing literature deals with various numerical methods and experimental techniques for investigating various problems in fluid mechanics. Therefore, a comprehensive review of the literature is neither necessary nor desirable and only a few references of particular interest will be mentioned here. Several surveys of the field of computational fluid mechanics are excellent, most notably the monograph by Roache[1] and his survey of the more recent literature.[2] A review of the early theoretical and experimental investigations of enclosed natural convection is given by Elder[3] and in an article by Ostrach.[4]

One of the first successful attempts at a numerical solution of a natural convection problem was conducted by Hellums and Churchill.[5] By developing a transient, explicit finite difference method, they obtained transient and steady-state solutions to the problem of natural convection on an isothermal vertical surface, a problem for which an exact solution exists. Their work also considered natural convection in a long horizontal cylinder having one vertical end heated and the other cooled. Wilkes and Churchill[6] extended the FDM of Hellums and Churchill to investigate the problem of thermally driven convection in a rectangular enclosure. In the ensuing 11 years, numerous investigators used the FDM to study similar internal free-convection problems for various geometries and parameters ranges. Notable among these is the work of Aziz and Hellums,[7] who first reported results on three-dimensional convection in a cubical cavity. Davis[8] and Rubel and Landis[9] formulated the enclosed rectangular problem in terms of a nonlinear fourth-order equation for the stream function without the explicit appearance of vorticity. Torrance[10] compared several FDMs that had been developed for examining natural convection flows and pointed out that the finite difference forms of the equations used by most previous investigators had not conserved energy or vorticity. Finally, Newell and Schmidt[11] examined the problem of enclosed, laminar natural convection over a range of parameters sufficient to determine a power-law correlation of the Nusselt number as a function of the Grashof number and aspect ratio. Larson and Viskanta[12] included the effects of radiation heat transfer on the enclosed convection problem.

The application of the finite-element method to the field of fluid mechanics is a fairly recent development, but has already produced an impressive body of literature. The recent survey article by Gartling[13] concerning the application of the FEM to viscous incompressible flow fields provides an overview of this area of current research. The general subject of the FEM is contained in the texts by Zienkiewicz[14] and Oden,[15] and a general review of applications to various fluid flow problems is discussed in Huebner.[16]

A sampling of the reported applications of the FEM to fluid mechanics indicates that much of the early work was directed primarily toward the problems of slow, viscous flow (creeping or Stokes flow). Atkinson et al[17] and Tong and Fung[18] achieved excellent results by employing the FEM and a fourth-order stream-function formulation to solve a number of channel flow problems. Thompson et al[19] formulated the problem in terms of primitive variables to solve creeping flows

both for Newtonian and for non-Newtonian fluids. The extension of the FEM to the more complex flow problems described by the Navier Stokes equations soon followed. Baker,[20] Cheng,[21] and Smith and Brebbia[22] used a stream-function/vorticity formulation of the governing equations to present successful solutions for isothermal flow problems involving a variety of geometries, including channel flows and flows over obstacles. A primitive variable approach was used by Oden and Wellford[23] to solve both transient and steady-state flows at low Reynolds numbers. Gartling and Becker[24] examined the steady-flow solution of both internal and external geometries. The addition of the energy equation to the FEM for determining the temperature field when the velocity and temperature fields are weakly coupled (e.g., forced convection) was demonstrated by the work of Hsu and Nickell,[25] Tay and Davis,[26] and Gartling,[27] among others.

When the flow and temperature fields are strongly coupled, as they are in natural convection, the FEM solution procedure necessarily changes. Most of the work reported to date has considered the time-independent form of the momentum and energy equations. Skiba, Unny, and Weaver[28] presented the first finite element solution to a free-convection problem (flow in a vertical slot). Since that time, Bedford and Liggett,[29] Young et al,[30] and Gartling[27] have demonstrated successful finite-element solutions for a variety of free-convection problems.

Optical methods of studying heat and mass transfer have been widely used for many years. The three main types of optical systems in common use are the shadowgraph, the Schlieren, and the interferometer. The visible indications of density variation for these methods depends, respectively, on the second derivative, on the first derivative, and directly on the index of refraction. The index of refraction of a gas is related to the density, and the density is related to the temperature through an equation of state (often the ideal gas law). Descriptions of the principles of operation of the above devices can be found in numerous texts (e.g., 31, 32).

In 1947 the English physicist Dennis Gabor introduced a radically new concept in photographic optics for which he later received the Nobel Prize in Physics (1971). This process, which can be called photography by wave-front reconstruction, is commonly known as holography. Holography does not record an image of the object being photographed but rather records the reflected light waves and an interfering reference beam. The resulting interference pattern forms a diffraction grating which, when illuminated by a similar monochromatic light beam, reproduces a three-dimensional image of the object. Extensive use of the procedure had to await the development of an intense monochromatic coherent light source, which Leith and Upatneiks[33] demonstrated in 1963 utilizing the newly developed laser. Following these developments, work in the field virtually exploded, resulting in over 800 papers by some 500 authors appearing in less than 10 years.[34] Holographic interferometry was one of the results of this widespread effort. A brief discussion of the basic principles involved can be found in References 35 and 36. Interpreting the data resulting from hologram interferometry (holometry) has proved to be reasonably difficult. Witte and Wuerker[37] appear to have been the first to demonstrate holometry as a quantitative measurement technique by determining (from an interpretation of the fringe pattern) the density profile through the gases

surrounding a high-speed projectile. Later, Matulka and Collins[38] were also successful in interpreting results both of axisymmetric and of asymmetric flow fields. More recent quantitative work includes that of Mayinger and Pankin[39] and Schimmel.[36]

It appears that, to date, no attempts to take advantage of the combined advances of various computational and experimental methods have been reported. This report is an effort to compare the results obtained from recently developed procedures for the problem of enclosed natural convection in several specified test geometries. With such a comparison we are then able to infer the validity of the respective techniques for this class of problems.

Computational Methods

The starting point for any numerical approach to the general problem of free convection is the mathematical description of the fluid motion through use of the basic conservation laws. If the fluid of interest is assumed to be incompressible within the Boussinesq approximation,[40] the basic field equations may be expressed as

Mass:
$$\frac{\partial u_i}{\partial X_i} = 0 \quad . \tag{1}$$

Momentum:
$$\rho \frac{\partial u_i}{\partial t} + \rho u_j \frac{\partial u_i}{\partial X_j} = \rho g_i + \rho g_i \beta \, (T - T_{ref}) + \frac{\partial \tau_{ij}}{\partial X_j} = 0 \quad . \tag{2}$$

Energy:
$$\rho C_p \frac{\partial T}{\partial t} + \rho C_p \, u_j \frac{\partial T}{\partial X_j} + \frac{\partial q_i}{\partial X_i} - S = 0 \quad . \tag{3}$$

The constitutive relations for the fluid consist of a Newtonian stress/rate-of-strain law,

$$\tau_{ij} = -P \, \delta_{ij} + \mu \left(\frac{\partial u_i}{\partial X_j} + \frac{\partial u_j}{\partial X_i} \right) \quad , \tag{4}$$

and Fourier's law for the heat flux,

$$q_i = -k_{ij} \frac{\partial T}{\partial X_j} \quad . \tag{5}$$

In Eqs. (1) through (5), u_i is the velocity component in the X_i coordinate direction, P is the pressure, T is the temperature, ρ is the density, τ_{ij} is the stress tensor, q_i is the heat flux vector, S is the volumetric heat source, μ is the viscosity, C_p is the heat capacity, k_{ij} is the thermal

conductivity tensor, and β is the coefficient of volume expansion. Also, T_{ref} is a reference temperature for which buoyancy forces are negligible, δ_{ij} is the unit tensor, and g is the gravitational constant. The above equations are expressed in terms of Cartesian coordinates; an analogous set of equations is available for axisymmetric geometries.

To complete the formulation of the boundary-value problem for convection, a suitable set of boundary and initial conditions is required. The hydrodynamic part of the problem requires that either the velocity components or the total surface stress (or traction) be specified on the boundary of the fluid domain. The thermal part of the problem requires that a temperature or heat flux be specified on the boundary of the energy transfer region. Symbolically, these conditions may be expressed by

$$u_i = f_i(s) \quad \text{on } \Gamma_u$$
$$t_i = \tau_{ij}(s)n_j(s) \text{ on } \Gamma_t \tag{6}$$

for the flow problem and

$$T = g(s) \quad \text{on } \Gamma_T$$
$$q_i(s)n_i(s) = h(s) \text{ on } \Gamma_q \tag{7}$$

for the heat-transfer problem. In Eqs. (6) and (7) the designation s is the coordinate along the boundary, n_j is the outward unit normal to the boundary, $\Gamma_f = \Gamma_u + \Gamma_t$ is the boundary enclosing the fluid, and $\Gamma_h = \Gamma_T + \Gamma_q$ is the boundary enclosing the energy-transfer region. For the transient problem, a set of initial conditions in the form of initial velocity and temperature distributions is also required.

Equations (1) through (5) along with the boundary conditions in (6) and (7) form a complete set for the determination of the velocity, pressure, and temperature fields in the fluid. A wide variety of numerical methods, already developed, allows this complex continuum problem to be reduced to a more manageable problem through some type of discretization procedure. In the following sections, descriptions of two such methods allow an approximate solution to the convection problem to be obtained.

Finite-Element Method

One of the approximate numerical methods being developed to treat general problems in convection is the finite-element method (FEM). Because, as noted, this very general approximation procedure has been thoroughly described by several authors, it is outlined only briefly here. A detailed description of the application of the method to free convection problems may be found in Reference 13.

The derivation of the finite-element equations begins with the division of the continuum region of interest into a number of simply shaped regions called finite elements. Within each element, a set of nodal points is identified at which the dependent variables (u_i, P, and T) are evaluated. Furthermore, the dependent variables are assumed to be expressable in the following form within each element:

$$
\begin{aligned}
u_i(X_i, t) &= \underset{\sim}{\Phi}^T(X_i) \cdot \underset{\sim}{u_i}(t) \\
P(X_i, t) &= \underset{\sim}{\Psi}^T(X_i) \cdot \underset{\sim}{P}(t) \\
T(X_i, t) &= \underset{\sim}{\Theta}^T(X_i) \cdot \underset{\sim}{T}(t) \ .
\end{aligned}
\tag{8}
$$

In Eq. (8) the designations $\underset{\sim}{u_i}$, $\underset{\sim}{P}$, and $\underset{\sim}{T}$ are vectors of unknown nodal point variables, and $\underset{\sim}{\Phi}$, $\underset{\sim}{\Psi}$, and $\underset{\sim}{\Theta}$ are vectors of interpolation or shape functions. The number of functions in a particular shape-function vector is equal to the number of nodes in an element at which the particular unknown is to be defined.

The approximations in Eq. (8) may be substituted into the field Eqs. (1) through (5) to yield a set of equations of the form

$$
\begin{aligned}
f_1(\underset{\sim}{\Phi}, \underset{\sim}{\Psi}, \underset{\sim}{\Theta}, \underset{\sim}{u_i}, \underset{\sim}{P}, \underset{\sim}{T}) &= \underset{\sim}{R_1} \\
f_2(\underset{\sim}{\Phi}, \underset{\sim}{u_i}) &= R_2 \\
f_3(\underset{\sim}{\Theta}, \underset{\sim}{\Phi}, \underset{\sim}{T}, \underset{\sim}{u_i}) &= R_3 \ ,
\end{aligned}
\tag{9}
$$

where R_i is the residual, or error, resulting from the use of the approximate forms for u_i, P, and T. A Galerkin procedure[15] may be used to reduce the errors, R_i, to zero in an average sense over each element by making the residuals orthogonal to the interpolation functions in Eq. 8. That is,

$$
\begin{aligned}
\langle \underset{\sim}{f_1}, \underset{\sim}{\Phi} \rangle &= \langle \underset{\sim}{R_1}, \underset{\sim}{\Phi} \rangle = 0 \\
\langle f_2, \underset{\sim}{\Psi} \rangle &= \langle R_2, \underset{\sim}{\Psi} \rangle = 0 \\
\langle f_3, \underset{\sim}{\Theta} \rangle &= \langle R_3, \underset{\sim}{\Theta} \rangle = 0 \ ,
\end{aligned}
\tag{10}
$$

where $\langle\ ,\ \rangle$ denotes the inner product defined by

$$\langle a,\ b\rangle = \int_v a \cdot b\, dv \quad ,$$

with v being the volume of the element.

When the procedure outlined above is carried out explicitly for the equations describing convection, the result is a set of coupled matrix equations of the form

$$\underset{\approx}{M}\dot{\underset{\sim}{V}} + \underset{\approx}{C}(\underset{\sim}{u})\underset{\sim}{V} + \underset{\approx}{K}\underset{\sim}{V} = \underset{\sim}{F}(\underset{\sim}{T}) \quad . \tag{11}$$

$$\underset{\approx}{N}\dot{\underset{\sim}{T}} + \underset{\approx}{D}(\underset{\sim}{u})\underset{\sim}{T} + \underset{\approx}{L}\,\underset{\sim}{T} = \underset{\sim}{G} \quad , \tag{12}$$

where

$$\underset{\sim}{U}^T = \left(\underset{\sim}{u}_1^T,\ \underset{\sim}{u}_2^T\right)$$

$$\underset{\sim}{V}^T = \left(\underset{\sim}{u}_1^T,\ \underset{\sim}{u}_2^T,\ P^T\right) .$$

The matrix equations in (11) and (12) represent the discrete analogs of the conservation equations for an individual finite element. The $\underset{\approx}{C}$ and $\underset{\approx}{D}$ matrices represent the advection (convection) of momentum and energy, respectively; the $\underset{\approx}{K}$ and $\underset{\approx}{L}$ matrices represent the diffusion of momentum and energy. The terms $\underset{\approx}{M}\dot{\underset{\sim}{V}}$ and $\underset{\approx}{N}\dot{\underset{\sim}{T}}$ represent the temporal acceleration and the heat capacity of the fluid; the $\underset{\sim}{F}$ and $\underset{\sim}{G}$ vectors provide the forcing functions for the system in terms of volume forces (body force, volumetric heating) and surface forces (stress, heat flux).

The discrete representation of the entire fluid region of interest is obtained through an assemblage of elements in such a way that interelement continuity of the approximate velocity, pressure, and temperature is enforced. This continuity requirement is met through the appropriate summation of equations for nodes common to adjacent elements.

Once the matrix equations for the finite element model have been assembled for the problem of interest, the task of solving this large set of strongly coupled, nonlinear equations still remains. In the present report only the case of steady-state flows will be addressed for the FEM. The matrix equations can, therefore, be reduced to

$$\underset{\approx}{C}(\underset{\sim}{u})\underset{\sim}{V} + \underset{\approx}{K}\,\underset{\sim}{V} = \underset{\sim}{F}(\underset{\sim}{T}) \quad , \tag{13}$$

$$\underset{\approx}{D}(\underset{\sim}{u})\underset{\sim}{T} + \underset{\approx}{L}\,\underset{\sim}{T} = \underset{\sim}{G} \quad . \tag{14}$$

The solution algorithm chosen for Eqs (13) and (14) consists of the following alternating procedure:

$$\underset{\approx}{D}(\underset{\sim}{u}^{n})\underset{\sim}{T}^{n+1} + \underset{\approx}{L}\,\underset{\sim}{T}^{n+1} = \underset{\sim}{G}$$

$$\underset{\approx}{C}(\underset{\sim}{u}^{n})\underset{\sim}{V}^{n+1} + \underset{\approx}{K}\,\underset{\sim}{V}^{n+1} = \underset{\sim}{F}(T^{n+1}) \qquad (15)$$

$$\underset{\approx}{D}(\underset{\sim}{u}^{n+1})\underset{\sim}{T}^{n+2} + \underset{\approx}{L}\,\underset{\sim}{T}^{n+2} = \underset{\sim}{G}$$

$$\vdots$$

etc.,

where the superscript indicates the iteration number. During observation of the behavior of this alternating solution scheme, it was apparent that most of the problems exhibited an oscillatory convergence. Therefore, an averaging scheme was used for the temperature field to speed convergence of the overall algorithm.

The finite element methodology developed in the previous sections has been incorporated into a Fortran coded computer program called NACHOS. This code is a highly modified and extended version of the fluid mechanics code TEXFLAP.[41]

The NACHOS code is organized in overlay form as shown in Figure 1. Communication between overlays is currently through low-speed disc files as noted in the figure. Input for the code, designed with the user in mind, has been kept to a minimum. An isoparametric mesh generator allows complex boundaries to be modeled easily and accurately. The present version of NACHOS requires approximately 160K words of storage on the Sandia Laboratories CDC 6600.

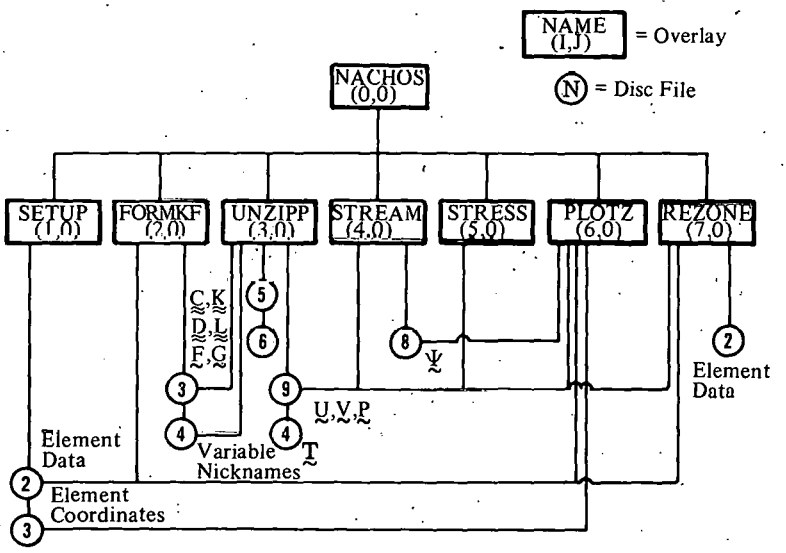

Figure 1. Organization of NACHOS Computer Code

The element library for NACHOS consists of an eight-node isoparametric quadrilateral and a six-node isoparametric triangle, as shown in Figure 2. Within each element, the velocity components and the temperature are approximated quadratically; the pressure is approximated linearly. The interpolation functions are from the "serendipity" family proposed by Erqatoudis et al.[42] The actual processing of the matrix equations is accomplished through a modified version of the frontal method developed by Irons.[43]

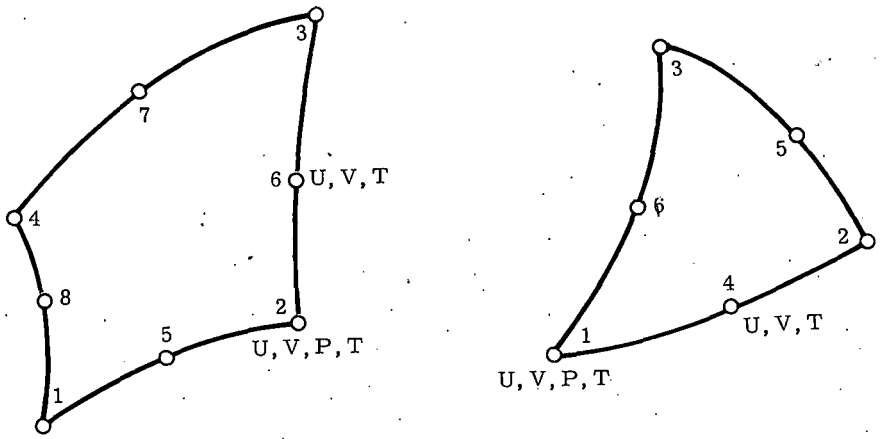

Figure 2. Isoparametric Finite Elements

Finite-Difference Method

The finite-difference method (FDM) to solving partial differential equations is to approximate the PDEs by suitable difference equations on a network of grid points, resulting in a set of algebraic equations. This traditional method is well established and documented in numerous texts.[44] The major concerns of the methods are accuracy, stability, convergence, and computational speed. The finite-difference methods that have been generally used in fluid mechanics problems are well documented in the treatise by Roache.[1] In general, the basic-difference methods may be conveniently divided into two classes: explicit and implicit.

The explicit schemes allow for the direct solution of the variable of interest by generating one algebraic equation and one unknown at each nodal point. Therefore, explicit methods are usually simpler and computationally faster than the implicit methods for a given step. However, explicit schemes usually have stringent grid size and time-step restrictions in order to obtain stable solutions. Most implicit schemes are unconditionally stable but computationally more complex, requiring the simultaneous solution of a system of equations. Both methods must satisfy certain conditions for the solution of the difference equation to also be a solution of the differential equation.[44, 45]

Equations (1) through (5) are coupled nonlinear partial differential equations, and considerable care must be used in their finite-difference representation if reasonably accurate results are to be obtained. For example, in writing Eq. (3), continuity has been used to simplify the equation. However, it can readily be shown that the standard forward, backward, or central difference representation of Eq. (3) does not conserve energy over the field.[10] It is necessary to write the advection terms in the nonexpanded form,

$$\rho C_p \frac{\partial(u_j T)}{\partial x_j} ,$$

to obtain a conservative difference representation; i.e., to conserve energy over the grid.

It is also very difficult to satisfy the finite-difference continuity equation when primary variables (u_i, P) are used. An alternative approach is to cross-differentiate and combine the x and y momentum equations to eliminate the pressure term and to introduce the stream function, ψ, which automatically satisfies continuity. This procedure replaces the continuity and momentum equations (1) and (2) with the vorticity (ω) and stream-function equations shown here:

$$\frac{\partial \omega}{\partial t} + \frac{\partial(u_i \omega)}{\partial x_i} = \nu\left(\frac{\partial^2 \omega}{\partial x_i^2} + \frac{\partial^2 \omega}{\partial x_j^2}\right) + g\beta \frac{\partial T}{\partial x_i} , \tag{16}$$

$$\omega = -\left(\frac{\partial^2 \psi}{\partial x_i^2} + \frac{\partial^2 \psi}{\partial x_j^2}\right) , \tag{17}$$

where

$$u_i \equiv \frac{\partial \psi}{\partial x_j} , \tag{18a}$$

$$u_j = \frac{-\partial \psi}{\partial x_i} , \tag{18b}$$

and

$$\omega \equiv \frac{\partial u_j}{\partial x_i} - \frac{\partial u_i}{\partial x_j} . \tag{19}$$

In difference form, it is frequently easier to solve Eqs. (3), (5), (16), and (17) than Eqs. (1) through (5); however, when these are properly formulated, the solutions will be identical.

For convective- and buoyancy-dominated situations, "upwind" differencing has been shown to enhance stability[10] and improve accuracy.[46] Accuracy is also improved for rapidly changing flow-field problems by allowing for an iterative procedure for the nonlinear (advection) terms, since during any one time step the terms are necessarily considered to be linear. Computational speed is frequently improved by solving for the temperature or the velocity field less frequently than for the other, depending upon the nature of the problem. For example, if the temperature field is changing rapidly while the flow field is changing relatively slowly, the flow field can be updated (solved) less frequently than the temperature field (energy equation) for a corresponding savings in computational time.

The solution procedure for the equations follows directly from the difference procedure used. An explicit formulation allows for the determination of the variable of interest at every point in terms of known quantities at the previous time step. A fully implicit formulation requires the simultaneous solution of the entire field. The resulting equations lead to a fully nonsymmetric matrix system with a bandwidth that depends on the geometry of the problem. The nonlinear terms and allowance of variable properties require the formation and inversion (or reduction) of the full matrix for every time step. This procedure is nearly always the most stable of the alternatives; however, it requires the largest amount of computer storage and is very involved computationally. Several methods are available for solving this full matrix system of equations.

The alternating-direction implicit (ADI) formulation requires two iterative sweeps for each time step, but the resulting system of equations leads (at least for regular geometries) to a tri-diagonal matrix system that requires little storage and is computationally very efficient.

The finite difference codes of this study use a stream function/vorticity formulation to solve for the coupled time-dependent velocity and temperature fields for a viscous, incompressible fluid flow. The codes are limited to the analysis of plane rectangular geometries or right cylinders of circular cross section. Equations (3), (16), and (17) can be written in nondimensional form by defining the following set of dimensionless variables:

$$U_i = u_i/u_o \qquad \theta = T/T_H$$

$$X_i = x_i/L \qquad \Psi = \psi/u_o L$$

$$\tau = tu_o/L \qquad \Omega = \omega L/u_o$$

$$u_o^2 = g\beta\Delta TL, \qquad Q = S/q_{ref}$$

and by introducing the dimensionless parameters

$$\text{Grashof number, } Gr = g\beta\Delta TL^3/\nu^2$$

$$\text{Prandtl number, } Pr = \nu/\alpha \ ,$$

where the variables are the same as those described previously and q_{ref} is a reference volumetric heating; T_H is a reference (boundary) temperature, and for an internally generating medium $T_H = q_{ref} L^2/k_{ij}$; ν is kinematic viscosity; α is thermal diffusivity; and L is a characteristic dimension.

Using the above definitions, we obtain the set of equations for the Cartesian geometry referred to as the dimensionless energy equation:

$$\frac{\partial\theta}{\partial\tau} + \frac{\partial(U_i\Omega)}{\partial X_i} = \frac{1}{Pr\sqrt{Gr}}\left(\frac{\partial^2\theta}{\partial X_i^2} + \frac{\partial^2\theta}{\partial X_j^2}\right) - Q = 0 \quad , \tag{20}$$

the dimensionless vorticity transport equation

$$\frac{\partial\Omega}{\partial\tau} + \frac{\partial(U_i\Omega)}{\partial X_i} = \frac{1}{\sqrt{Gr}}\left(\frac{\partial^2\Omega}{\partial X_i^2} + \frac{\partial^2\Omega}{\partial X_j^2}\right) + \frac{\partial\theta}{\partial X_i} \quad , \tag{21}$$

the dimensionless stream function equation

$$\Omega = -\left(\frac{\partial^2\Psi}{\partial X_i^2} + \frac{\partial^2\Psi}{\partial X_j^2}\right) \quad , \tag{22}$$

and the dimensionless velocity equations

$$U_i = \frac{\partial\Psi}{\partial X_j} \quad , \quad U_j = \frac{\partial\Psi}{\partial X_i} \quad . \tag{23}$$

The temperature boundary conditions are the same as those discussed previously, Eq. (7), expressed in dimensionless form. The stream-function boundary conditions are a zero (or constant) condition and a zero normal gradient condition at the wall. The initial velocity, temperature, vorticity, and stream-function conditions must also be prescribed; usually they are initialized in natural convection problems as a zero condition. The boundary condition on vorticity is obtained indirectly during the problem solution. Using a Taylor series expansion of the stream function in the vicinity of the wall and noting from the stream-function equation (22) with its boundary conditions that $\Omega_o = \partial^2\Psi/\partial X^2$, we obtain a second-order approximation for the wall vorticity from the interior function,

$$\Omega_o = -(8\Psi_1 - \Psi_2)/2(\Delta X)^2 \quad , \tag{24}$$

where subscripts 1 and 2 represent values removed one and two grid points from the wall and Δx is the grid spacing.

The codes use an ADI solution scheme with conservative upstream differencing. The rectangular geometry also allows for finite-thickness heat-conducting walls and radiative transfer within the enclosure.[12] The solution scheme consists of advancing the temperature through a time step by solving Eq. (20). The vorticity transport equation (21) is then solved for all interior (nonboundary) nodal points. Next, the stream-function equation (22) is solved by converting it to a time-dependent (parabolic) equation and using an ADI scheme until the time-dependent term is equal to zero. From the solution of the stream-function equation, the wall (boundary) vorticities are then updated by using Eq. (24), and the velocity field, Eq. (23), at the end of the time step is determined.

The two finite difference codes (rectangular and cylindrical) are time efficient, and typical run times for small problems are less than 300 seconds on a CDC 6600 computer for a full transient solution of an enclosed natural convection problem. The efficiency of the code, however, also extracts a penalty in generality. The geometry limitations with regular mesh spacing appears to be the most restrictive condition for solving many problems of interest.

Experimental Method

For the purpose of this paper, holography can be considered a technique for reproducing in its entirety a visual image of an object or of a region in space. This image preserves all the optical features of the object or space including its three dimensionality. It is primarily a method of reconstructing a virtual image by recording the radiated coherent light reflecting from an opaque object or the transmitted light that passes through a transparent medium. This coherent radiation which contains important phase and amplitude information, is referred to as the object beam (Figure 3). At the hologram, which is usually a high-resolution photographic plate, the object beam is combined with the off-axis coherent radiation referred to in the figure as the "reference beam." The photographic emulsion records the complex interference pattern, formed as a result of the coherent superposition of the two wavefronts. In this regard, holography is similar to classical interferometry except that, because of the spatial coherence of the laser, the two beam lengths need not be exactly equal. After the hologram is photographically processed, it will, when viewed with incoherent light, bear no resemblance to the original objects. It will contain a high-frequency (microscopic) interference pattern that can be considered a generalized diffraction grating. When this grating is reilluminated with the reference beam (or any other expanded beam produced by the same type of laser), it will refract the light in a systematic manner that reconstructs all the phase and amplitude information of the original object beam. This reconstructed wavefront can then be processed by an image-forming system, such as a camera, to make a permanent record of the virtual image.

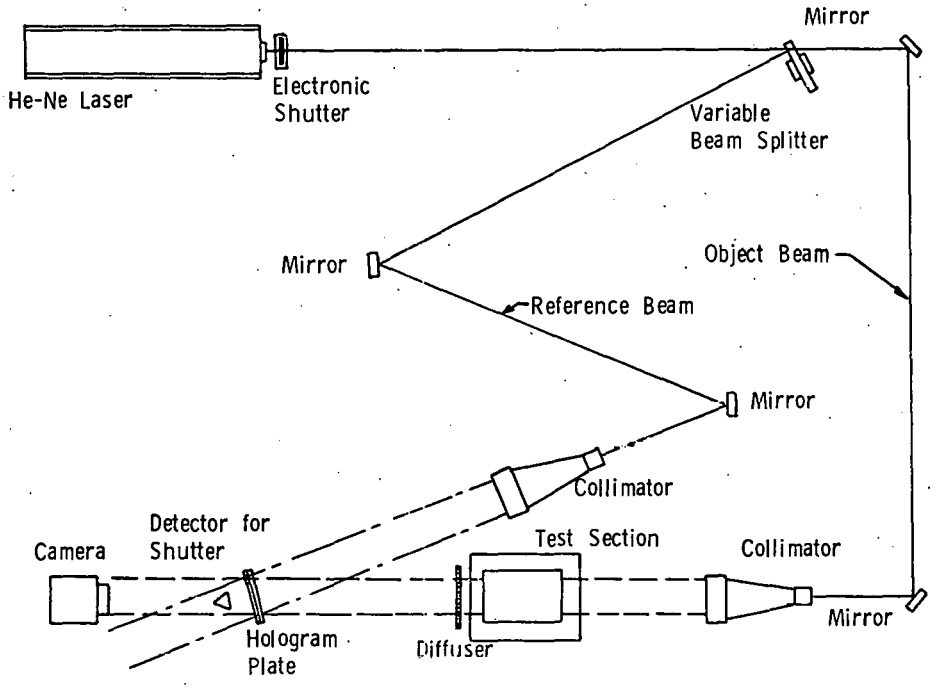

Figure 3. Laser Holometric Setup, Schematic

Holometry, or hologram interferometry, is a simple extension of the reconstruction process described above. Because the hologram permits reconstruction of an object wavefront at some later time, it is possible to have the reconstructed wavefront interfere with another real-object wavefront. In this process, known as "real-time" holometry, fringes will form whenever the instantaneous object beam deviates in phase from its original state by an appropriate amount. Original state, of course, refers to the condition under which the hologram was initially exposed. One point that should be made about this technique is that the hologram must be very carefully repositioned after photographic processing; otherwise, displacement fringes will result. Attempts to prevent faulty positioning have led to a host of hologram holders, including some that process "in situ" to avoid moving the plate. Actually, because the photographic emulsion can shift with respect to the plate, some of these devices use a fluid gate to precondition the emulsion.

Alternatively, it is possible to record the object twice during different states and to reconstruct the two object wavefronts simultaneously at a later time. Again, all that is required for viewing the interference pattern is that the beam be produced by the same type of laser. This is the so-called double-exposure method, because the hologram is exposed twice before processing. A direct analog exists in classical interferometry, provided that the instrument is adjusted for the "infinite-fringe," or uniformly bright screen. One of the disadvantages of this double-exposure method is that fringes correspond to quantum shifts in index of refraction and are therefore widely spaced. It would be better to have a pattern of tightly spaced fringes so that the density gradients could be deduced from fringe gradients. This can be accomplished in real-time holometry by

deliberately introducing a series of displacement fringes in such a way that they form the desired tightly spaced pattern. No such capability exists in the double-exposure method.

The components of the present holometric system are shown in schematic form in Figure 3. The entire arrangement is isolated from building vibrations by a Modern Optics V-12 stable-table system with viscous mechanical dampening. Dimensions of the table top are 122 x 213 cm, and flatness is certified to ±0.04 mm overall. Resonant frequency of the air-mount system is less than 1.25 Hz. Illumination of the system is provided by a Spectra-Physics Model 125-A helium/neon laser with RF excitation. The laser is claimed to be a 50-mW TEM_{∞} at 632.8 nm, but careful alignment of the cavity has resulted in an output of approximately 80-90 mW at the exit mirror.

A typical mirror mount consists of a magnetic stand, mirror, and positioning holder. The mirrors are all $\lambda/10$ at 632.8 nm with spectral reflectances of 95 percent or better (45° incidence). The variable beam splitter is a Jodon Model VBA-200, capable of continuously varying the transmitted beam from 0.7 to 90 percent and the reflected beam from 8.5 to 85 percent. Expansion of the object and reference beams is accomplished by a pair of Tropel Model 280-100A laser beam collimators with 100-mm exit optics and 1.5-mm entrance apertures. The collimator holders were assembled from standard optical table hardware.

The electronic shutter system is a Jodon Model ES-100, used in the integrating exposure mode with the power density detector located behind the hologram plate (Figure 3). Because Agfa-Gaevert 10E75 4 x 5 glass plates were the only plates used in this preliminary work, the shutter system was calibrated to permit an exposure of approximately 50 ergs/cm^2. In the double-exposure runs, each exposure was one-half this amount. The camera used to record the resulting interferograms is a Rolleiflex SL-66, 6 x 6 cm single-lens reflex, usually used with a 150-mm f4.0 lens. Except for preliminary work, all photographs were taken with Polaroid Type 105 black and white P-N film. The negatives were then analyzed on a Gaertner toolmaker's microscope with substage illumination. Translation of the negative in the x and y directions (fringe spacing) can be measured to about 2.5 μm.

The various test sections used in this preliminary study were mounted on an interferometrically stable laboratory jack. To monitor surface and ambient temperatures, we read a series of chromel/alumel thermocouples on an Ohmega Model 415 digital temperature indicator. The device uses an internal cold junction, and a temperature resolution of the order of 0.1 K is claimed by the manufacturer. A photograph of the complete holometric setup is presented in Figure 4.

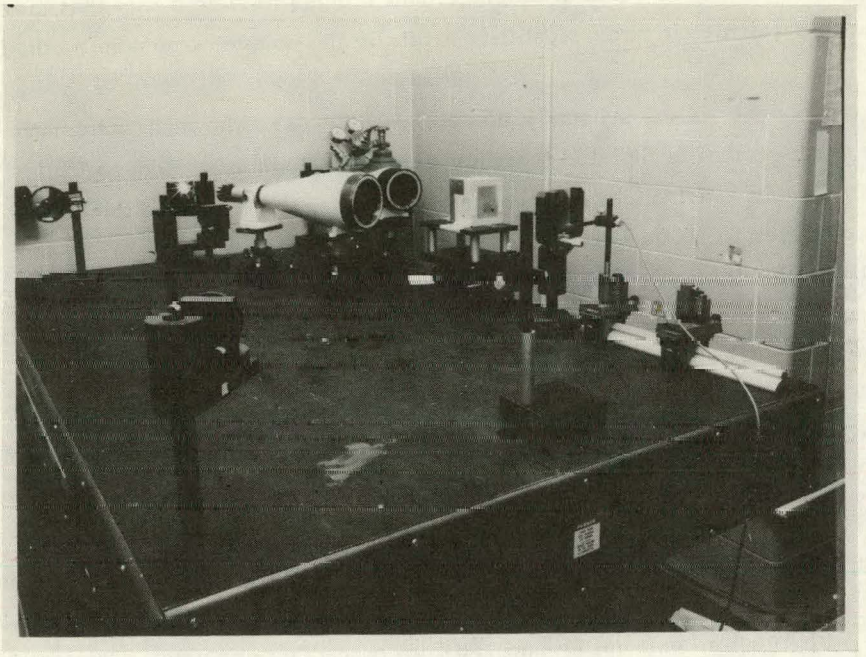

Figure 4. Laser Holometric Setup, Photograph

Results and Comparisons

A large number of problems have been examined by means of the FDM and FEM codes, and only a small sampling of the problems is included here. The example problems have been chosen either to demonstrate a unique analysis capability (e.g., computation of combined radiation and convection) or to provide a focal point for the comparison of the different techniques. The first two examples illustrate results from the numerical analysis; the latter two show results from both the experimental work and the numerical procedures.

Free Convection Due to a Local Heat Source

As a first example, the finite-difference code was used to examine the transient thermal response of a rectangular enclosure to a local hot spot centered on the bottom. Figure 5 shows the development of the isotherms, including radiative heat transfer, at four dimensionless times for a Grashof number of 10^6. The alternate light and dark fields represent 10-percent increments of temperature from θ_{min} to θ_{max}, where $\theta_{max} = 1$ at the hot spot. The external surfaces of the horizontal walls are assumed to be insulated, and the vertical walls are assumed to have convective transfer to ambient air. Figure 6 shows the same problem but with radiative heat transfer neglected. For this problem, the effect of radiation is very pronounced (as seen also in Figure 7, which shows the temperature profile at enclosure midheight for the two conditions at near steady-state conditions).

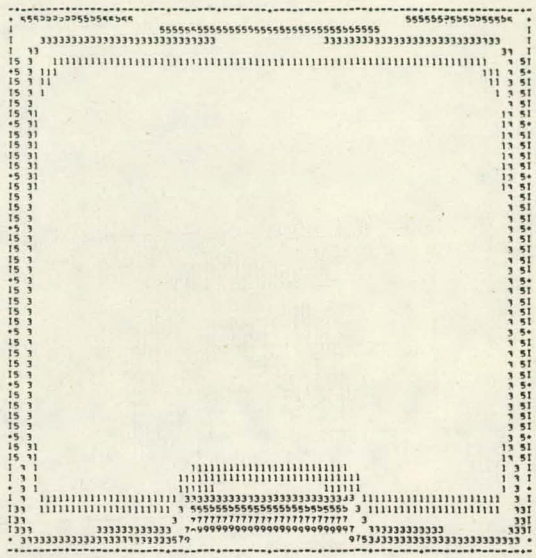

(a) $\tau = 1.5$, $\theta_{min} = 0.30$

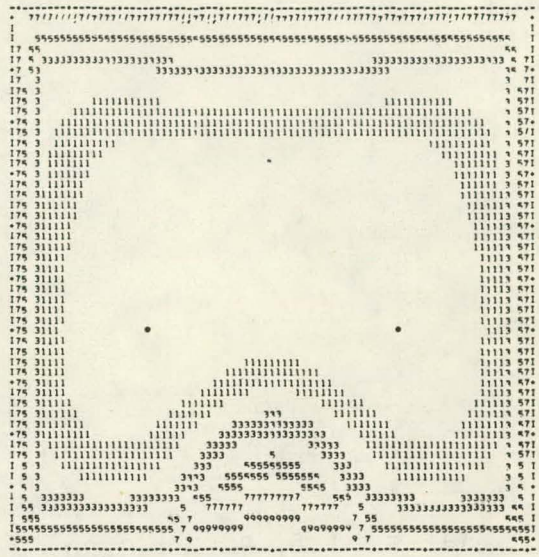

(b) $\tau = 5.0$, $\theta_{min} = 0.30$

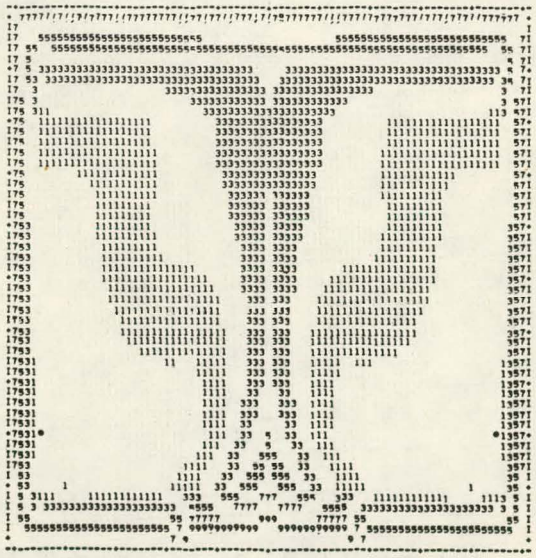

(c) $\tau = 10.0$, $\theta_{min} = 0.42$

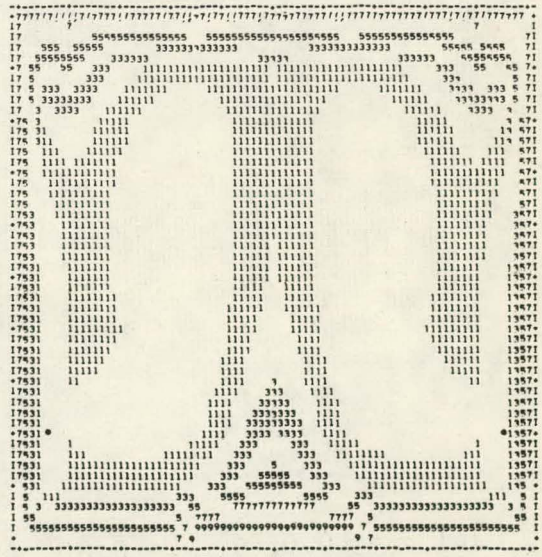

(d) $\tau = 15.0$, $\theta_{min} = 0.53$

Figure 5. Transient Isotherms for Local Hot Spot on Floor, Gr = 10^6, FDM

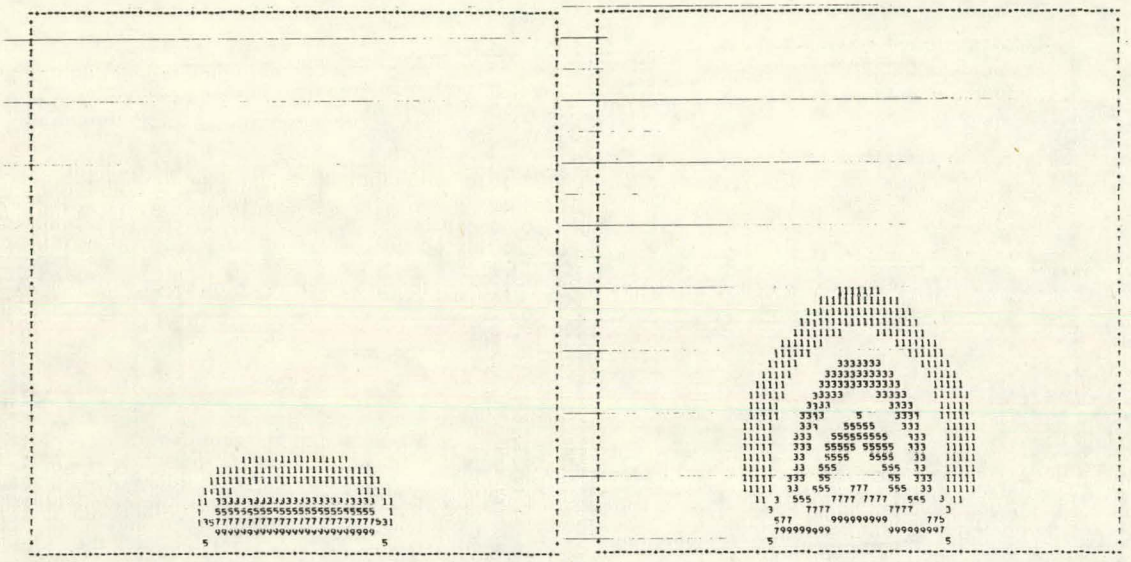

(a) $\tau = 1.5$, $\theta_{min} = 0.30$ (b) $\tau = 5.0$, $\theta_{min} = 0.30$

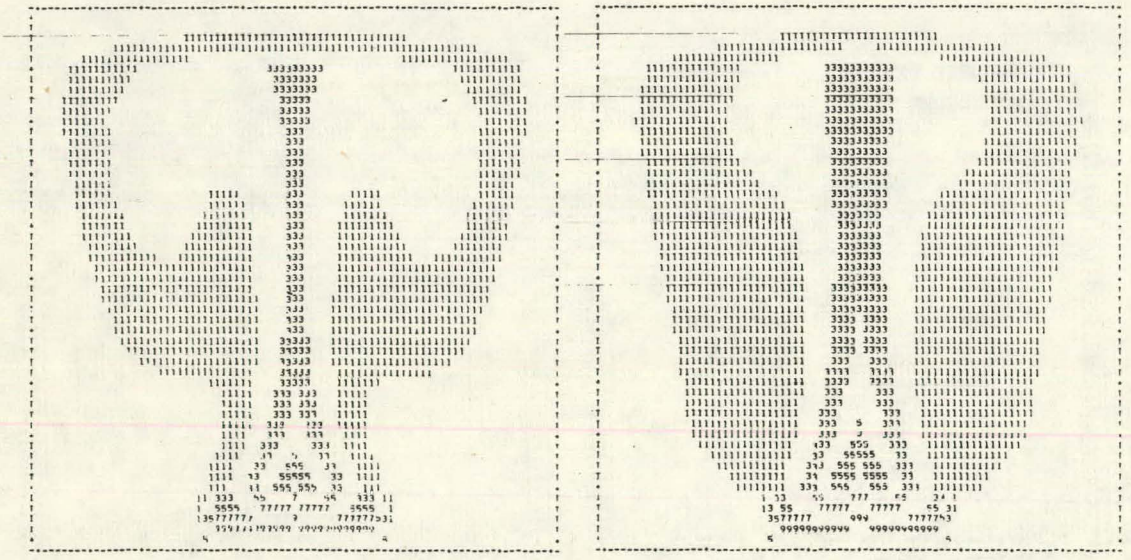

(c) $\tau = 10.0$, $\theta_{min} = 0.30$ (d) $\tau = 15.0$, $\theta_{min} = 0.30$

Figure 6. Transient Isotherms for Local Hot Spot on Floor Neglecting Radiant Heat Transfer, Gr = 10^6, FDM

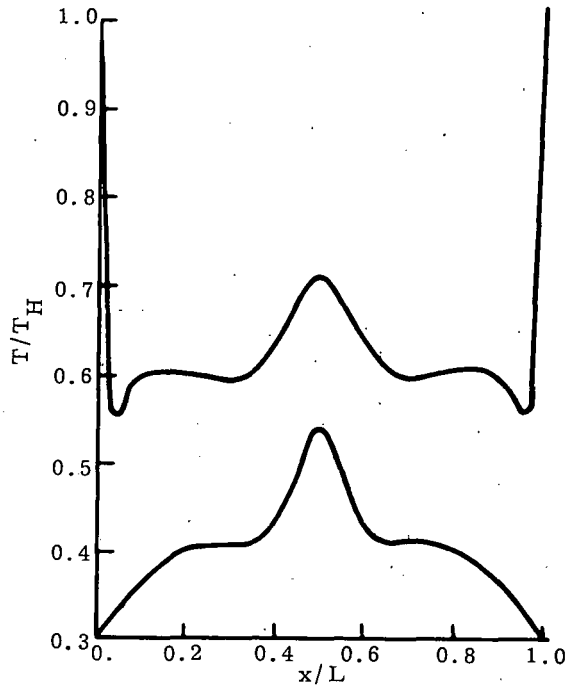

Figure 7. Temperature Profile at Enclosure Midheight (y/H = 0.5) for Local Hot Spot on Floor, τ = 20, Gr = 10^6, FDM

Free Convection Due to Volumetric Heating

To obtain a quantitative comparison between the two numerical methods, we considered the conceptually simple problem of a volumetrically heated fluid in a vertical cylindrical enclosure. The cylindrical container was assumed to be insulated along the top and bottom surfaces; the vertical surface was maintained at a constant temperature. The enclosed fluid was assumed to be producing heat volumetrically so that the modified Grashof number ($Gr^* = g\beta SL^5/\nu^2 k$) was 1×10^6. The Prandtl number was 0.71.

The finite-difference code used a uniformly spaced 21 x 21 grid and followed the transient behavior of the fluid until a steady state was reached. The finite-element code, which employed a nonuniform 10 x 10 element grid, solved for the steady state directly. The results of these computations are shown in Figures 8 through 11.

Figures 8 and 0 illustrate the streamlines and isotherms computed by the two methods. The qualitative agreement is seen to be excellent (the maximum difference between the codes for any variable was less than 5 percent). This quantitative agreement can be easily seen in Figures 10 and 11, where vertical velocity and temperature are plotted versus enclosure radius at a midheight position in the cylinder. The finite-difference code used 192 seconds of CPU computer time, and the finite-element code used 430 seconds.

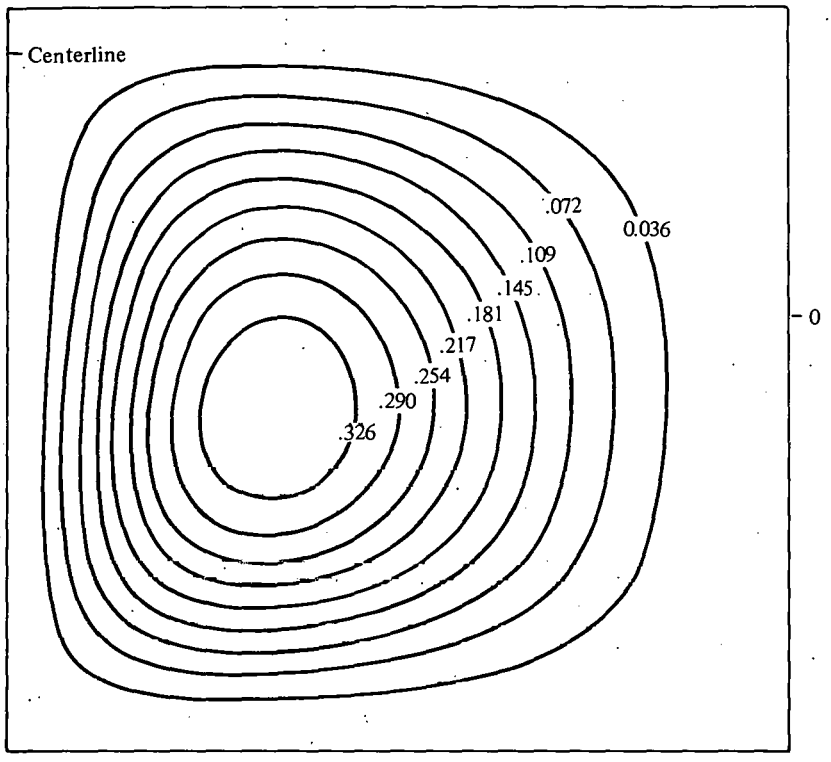

a. FDM

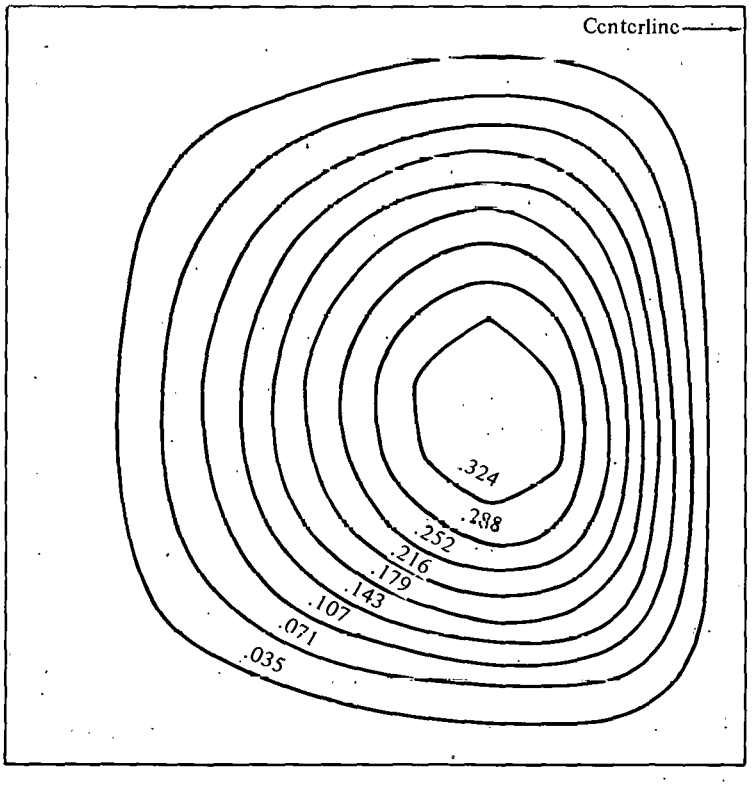

b. FEM

Figure 8. Streamlines in a Volumetrically Heated Vertical Cylinder

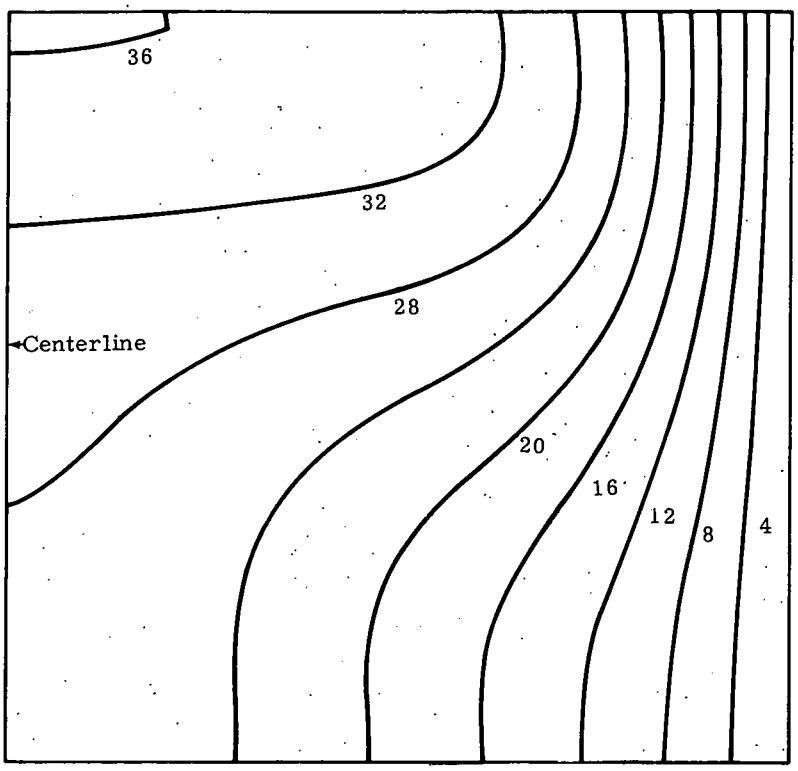

a. FDM

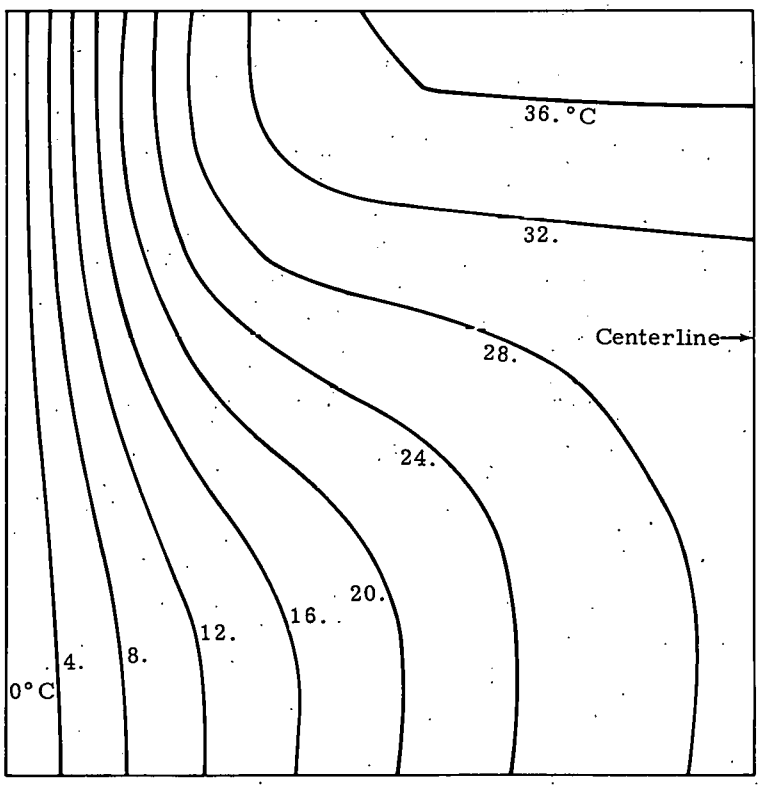

b. FEM

Figure 9. Isotherms in a Volumetrically Heated Vertical Cylinder

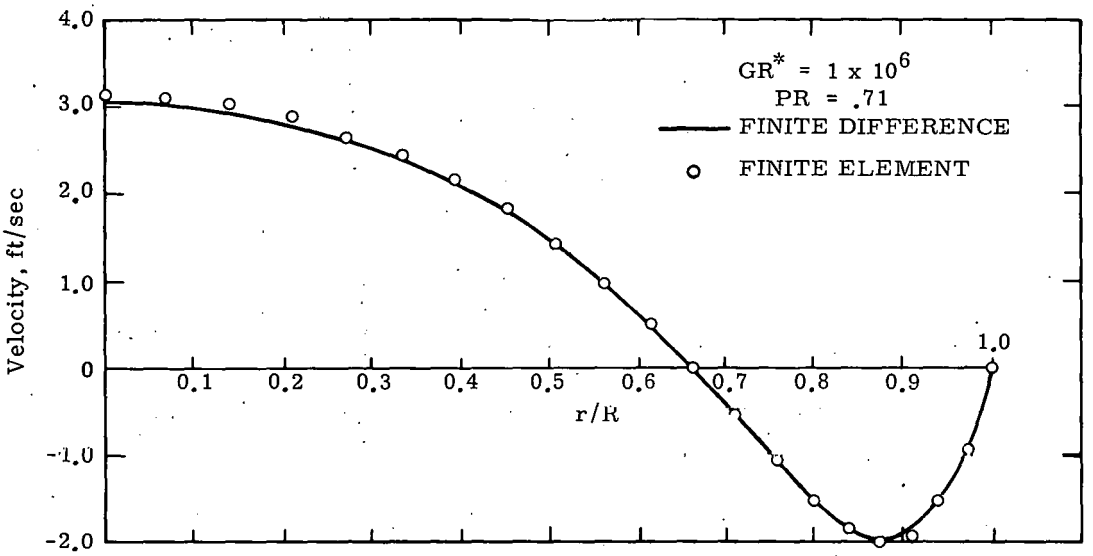

Figure 10. Predicted Velocity Profile at Enclosure Midheight in a Volumetrically Heated Vertical Cylinder

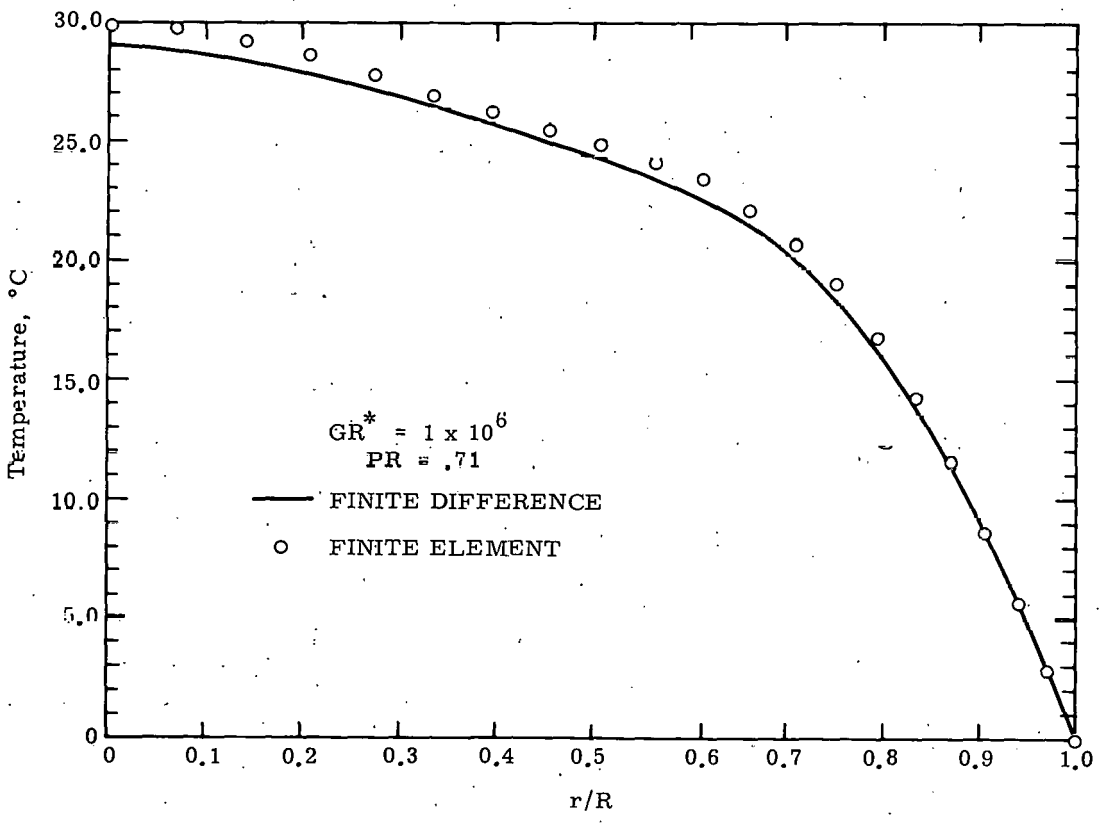

Figure 11. Predicted Temperature Profile at Enclosure Midheight in a Volumetrically Heated Vertical Cylinder

Free Convection in Rectangular Enclosures

This section presents the results for two geometric configurations that were analyzed both experimentally and numerically.

The first configuration examined was a heated horizontal right circular cylinder in an isothermal rectangular cross-section box, as shown in Figure 12. A transparent glass plate covered the entrance end of the box (with respect to the laser beam) and a ground-glass plate formed the exit-end boundary. Note that the 2.8-cm-diameter cylinder is affixed to a phenolic stand, which provides stability to the cylinder and acts as a thermal insulator between the cylinder and box. Thermocouples were mounted on the inside of the cylinder next to the electrical heating coil and on the outer surface between the cylinder and the stand. The heater and thermocouple leads were routed to the rear of the cylinder as shown in the figure. The surrounding box was constructed of 1.9-cm-thick aluminum plate. Cross hairs on the entrace and exit planes helped in the alignment process. The opening in the box was 6.4 x 8.9 cm, and the inside was painted flat black to minimize reflection. A second configuration, in which the right circular cylinder was replaced by a heated hexagonal cross-section cylinder, was also examined. The components for this test section are shown in Figure 13.

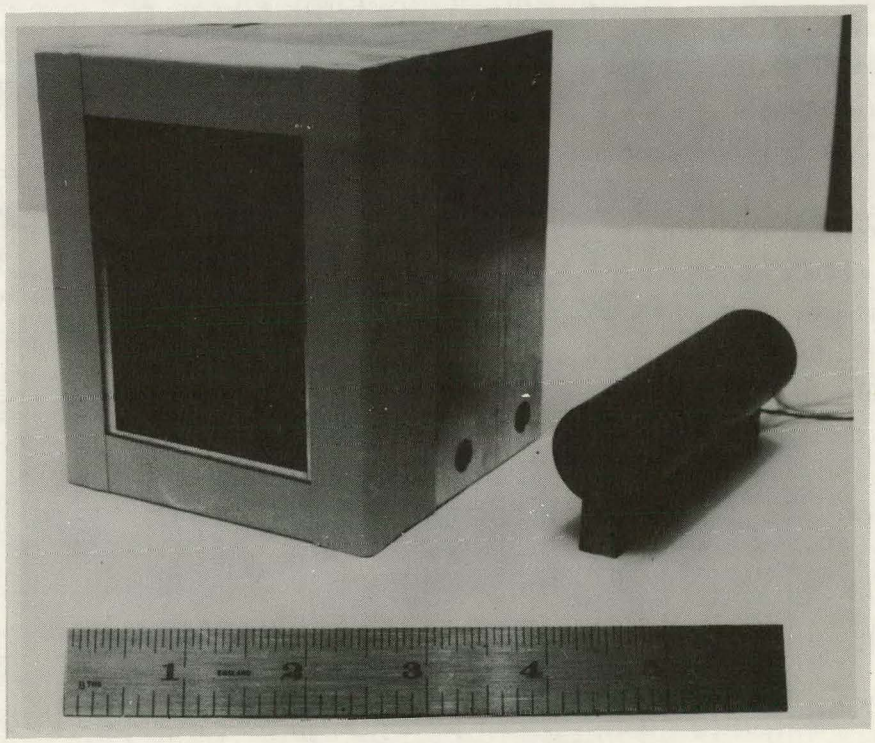

Figure 12. Test Section 1, Heated Horizontal Cylinder in an Isothermal Rectangular Box

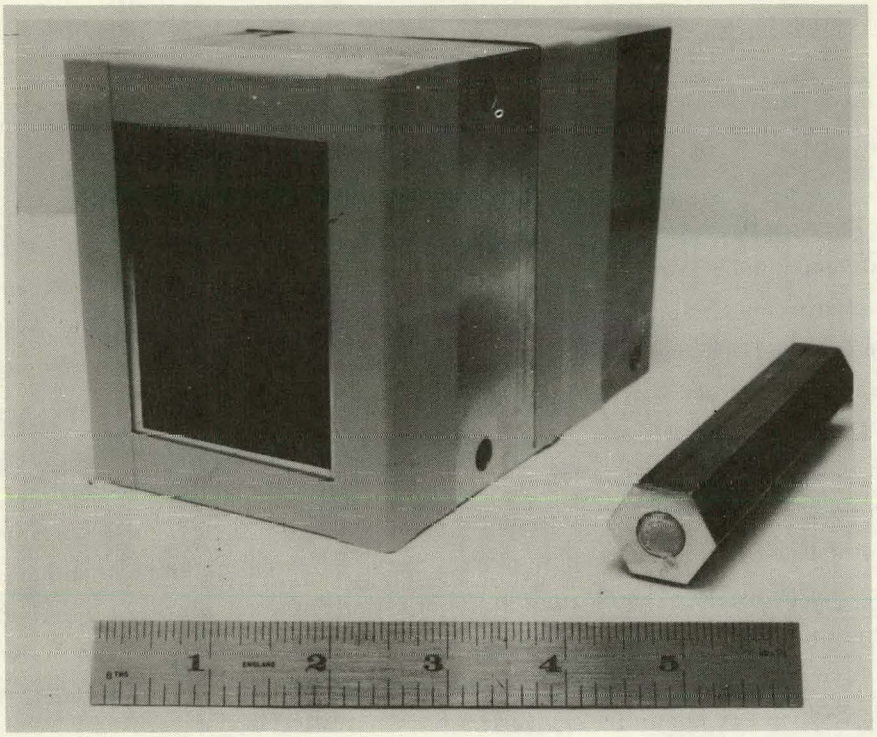

Figure 13. Test Section 2, Heated Hexagonal Cylinder in an Isothermal Rectangular Box

The two experimental configurations were also analyzed by mean of the finite-element code; furthermore the finite-difference code was employed on the hexagonal cross-section cylinder geometry. Typical computational meshes for both geometries are shown in Figures 14 and 15.

The configuration of the heated circular cylinder in the isothermal rectangular cross-section box produced the double-exposure holometrogram (holometric interferogram) presented in Figure 16. The cylinder surface temperature was determined to be 351.5 K, and the box temperature was 294.3 K. Use of the data-reduction technique outlined in Reference 36 indicates that there should be six fringes. The photograph clearly confirms this prediction. Temperatures corresponding to the fringes are as follows:

ϵ	T (K)	$T - T_1$ (K)
Cold Surface	294.3	0
1	302.4	8.1
2	311.0	16.7
3	320.0	25.7
4	329.6	35.3
5	339.8	45.5
6	350.7	56.4
Hot Surface	351.5	57.2

Because of the preliminary nature of this study, no attempt was made to deduce heat-transfer coefficients for this configuration.

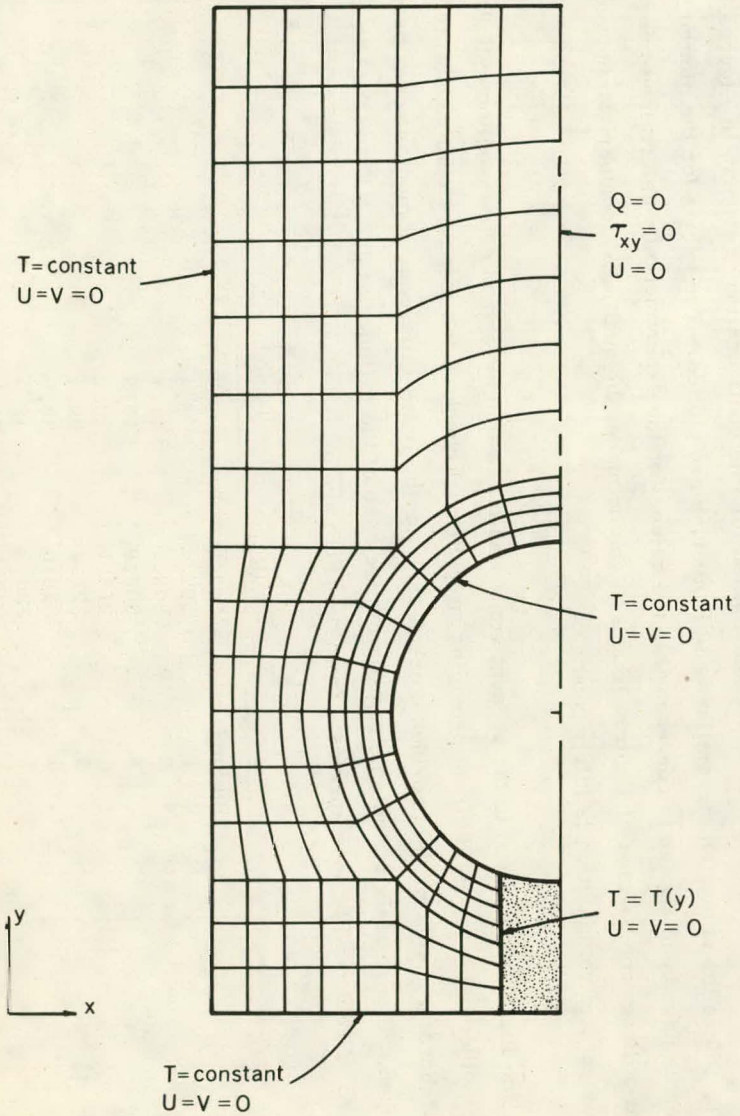

Figure 14. Finite Element Mesh for Configuration of Test Section 1

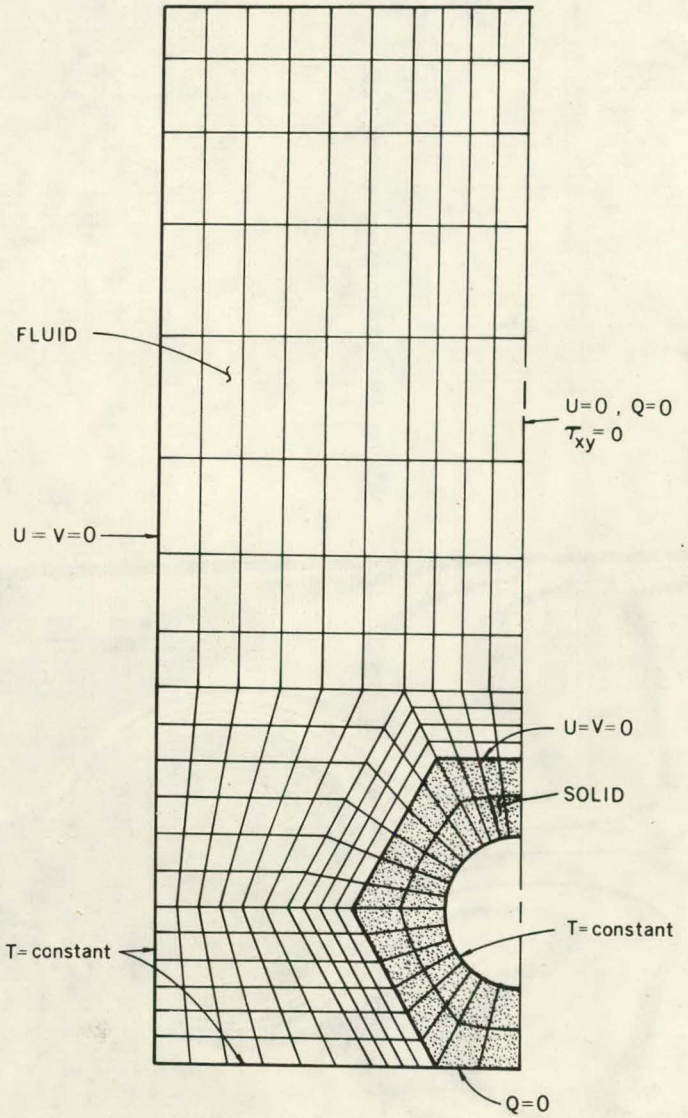

Figure 15. Finite Element Mesh for Configuration of Test Section 2

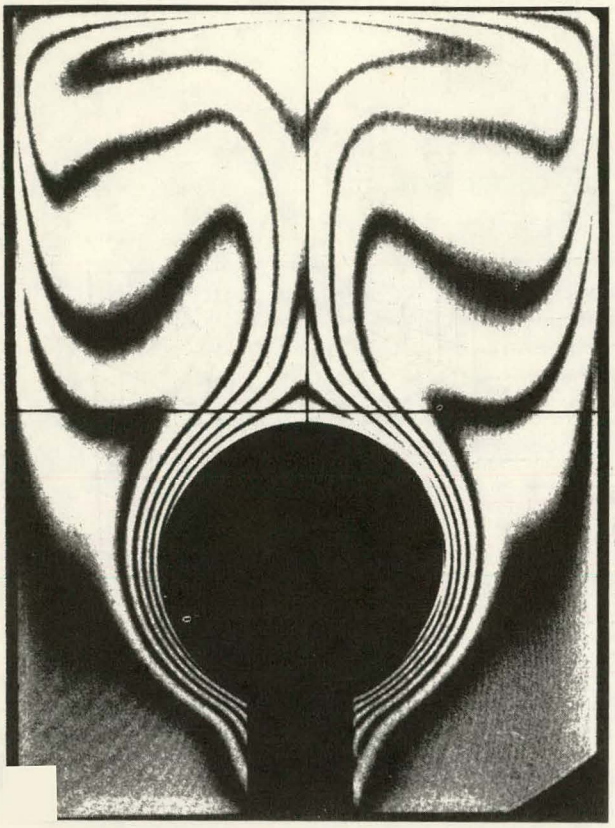

Figure 16. Holometrogram of Test Section 1

The results of the finite-element computation for this configuration are shown in Figures 17 and 18, where the computed streamlines and isotherms are plotted. The values for the plotted isotherms have been chosen to correspond to the values for the experimentally determined fringes so that a direct comparison of Figures 16 and 18 can be made; the qualitative comparison between experiment and computation is fairly good.

The final test case run in the present study was the heated hexagonal cross-section cylinder in the isothermal box. Aside from providing an additional check on the measurement capability of the laboratory, this model provides a check case for the finite-difference computer codes being developed. Figure 19 is the holometrogram for the case of the cylinder at 358.1 K and the box at 292.0 K. Fringe and temperature data from the photo are given below:

ϵ	T (K)	$T - T_1$ (K)
Cold Surface	292.0	0
1	297.4	5.4
2	303.1	11.1
3	308.9	16.9
4	315.1	23.1
5	321.4	29.4
6	328.0	36.0
7	334.9	42.9
8	342.1	50.1
9	349.6	57.6
10	357.4	65.4
Hot Surface	358.1	66.1

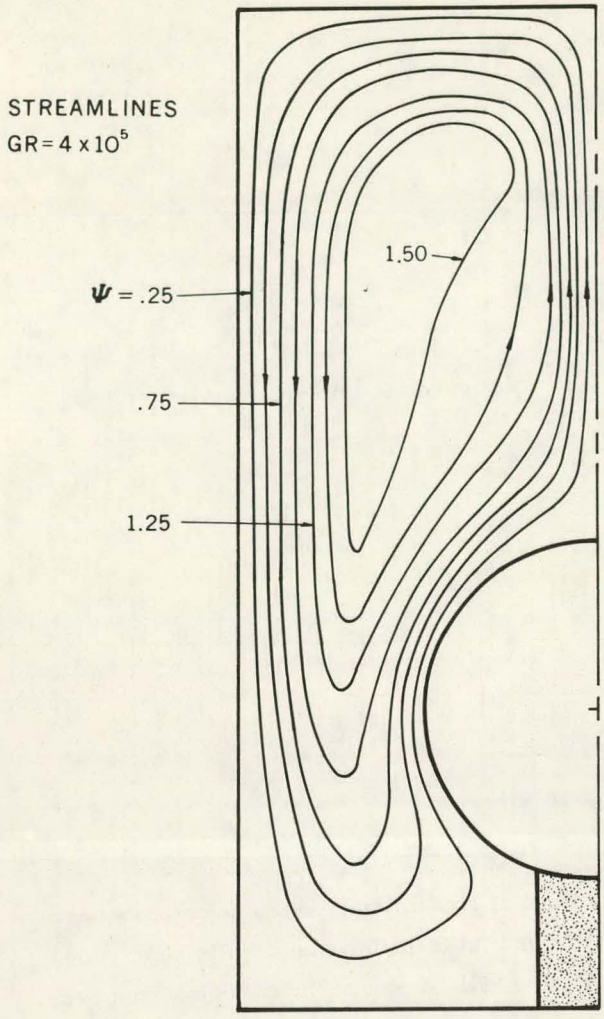

Figure 17. Predicted Streamlines for Test Section 1, FEM

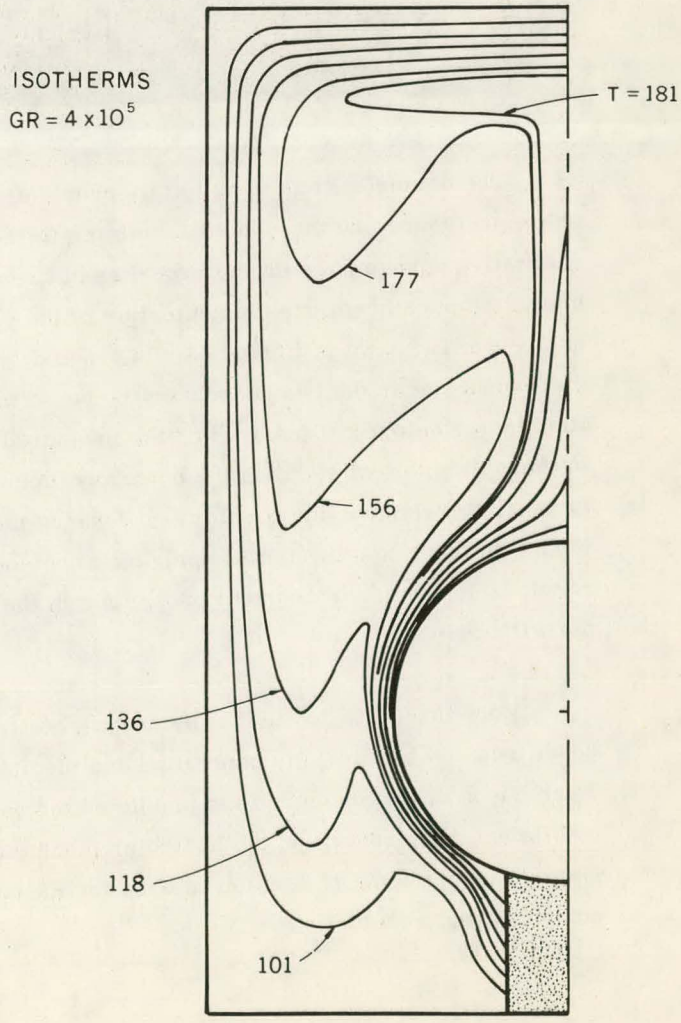

Figure 18. Predicted Isotherms for Test Section 1, FEM

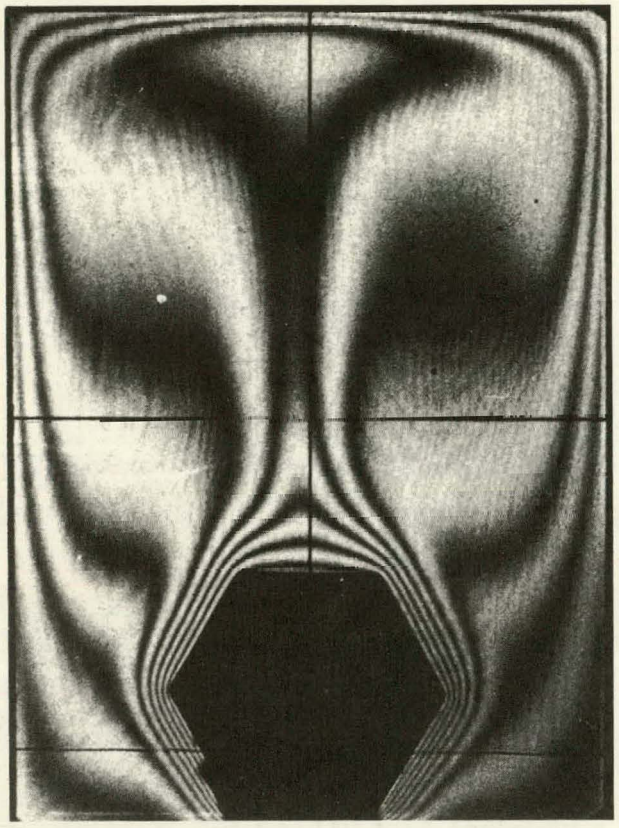

Figure 19. Holometrogram of Test Section 2

The numerical solutions to this problem, in the form of streamline and isotherm plots, are shown in Figures 20 through 23. Both the finite-element and finite-difference results show good qualitative agreement with the experimental results (Figure 19). A plot of the measured and predicted temperature along the centerline of the plume (from the top of the hexagon to the top of the enclosure) is shown in Figure 24. In general, the agreement is within 10 percent. Some of the discrepancy near the two boundaries is due to the parallax effect of the photograph (made from the illuminated hologram) from which the measured data are taken. Another source of error is that in these simple test sections the boundary temperatures were not truly isothermal, as was assumed in the finite-element and the finite-difference models; however, the temperature was not monitored in enough positions to warrant applying a nonisothermal boundary to the models. Further disparities result from the use of constant properties in the models and from variations between the FEM and the FDM grids.

More sophisticated test cells are currently being designed and assembled so that the boundary conditions can be carefully controlled and monitored. This will allow a more detailed quantitative comparison of the measured and predicted temperature distribution (and resulting heat-transfer coefficient distribution) on the heated element and surrounding enclosure. In addition, a laser/Doppler velocimeter is being developed for measuring the velocity field to compare it with the computational results.

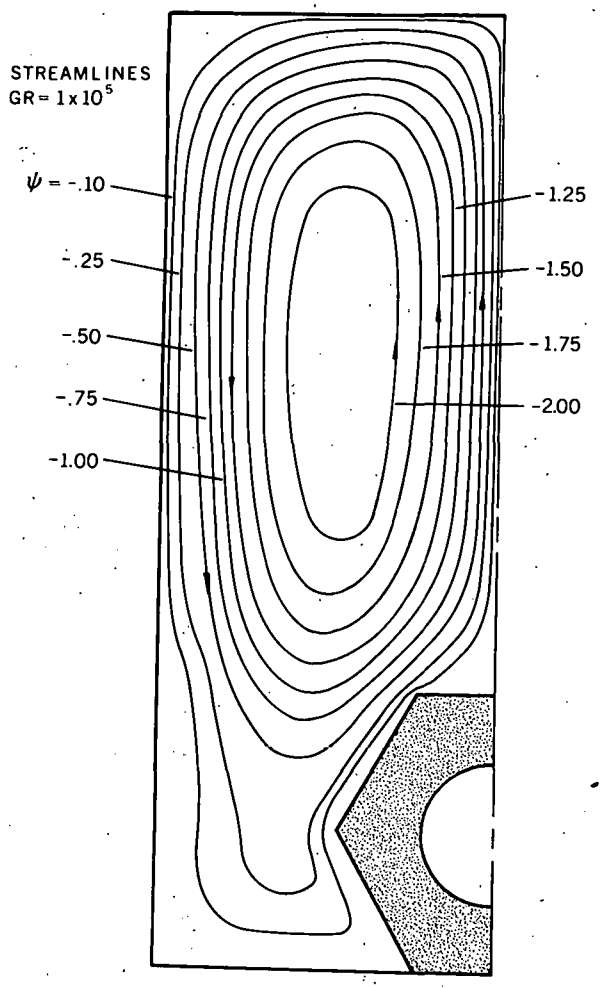

Figure 20. Predicted Streamlines for Test Section 2, FEM

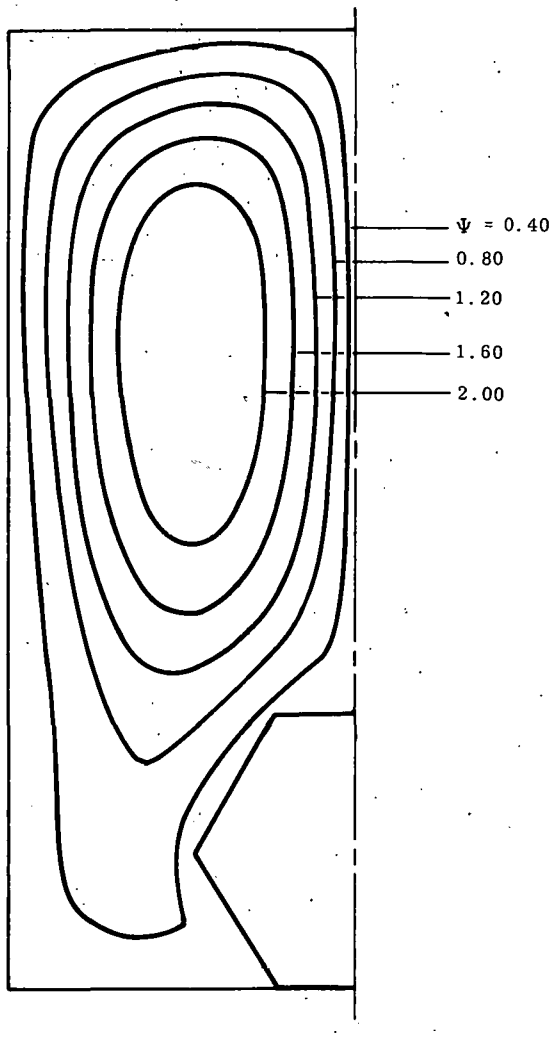

Figure 21. Predicted Streamlines for Test Section 2, FDM

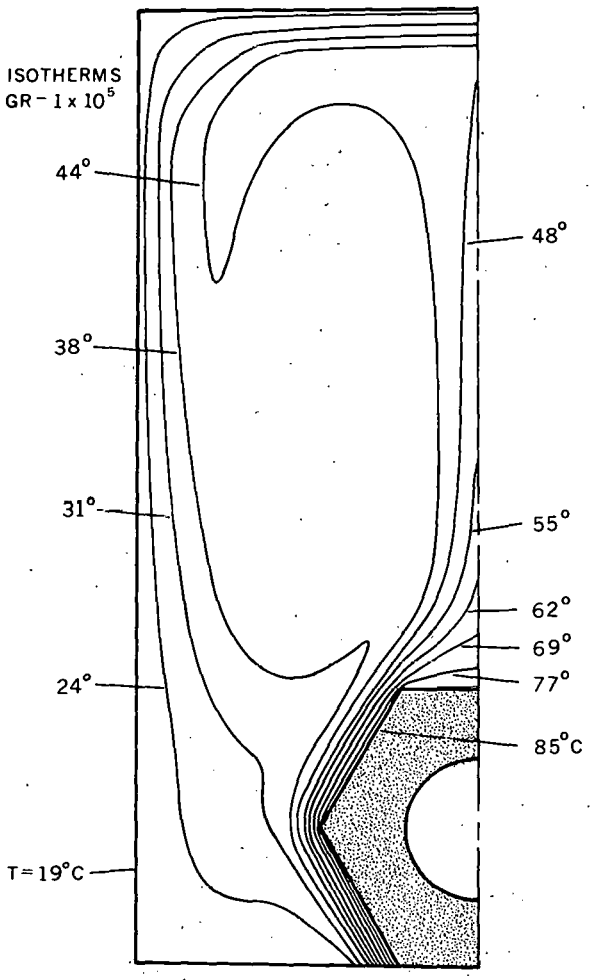

Figure 22. Predicted Isotherms for Test Section 2, FEM

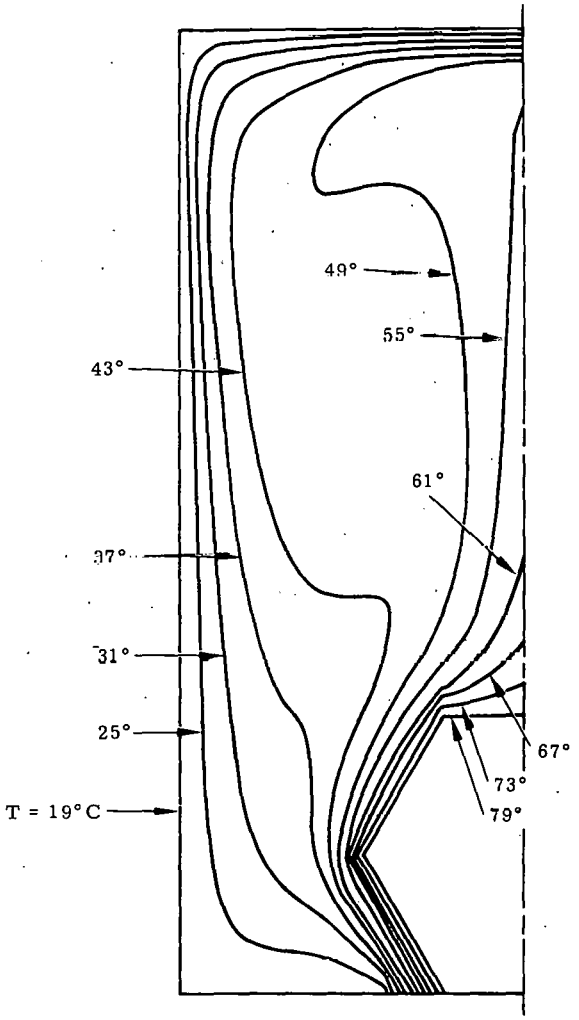

Figure 23. Predicted Isotherms for Test Section 2, FDM

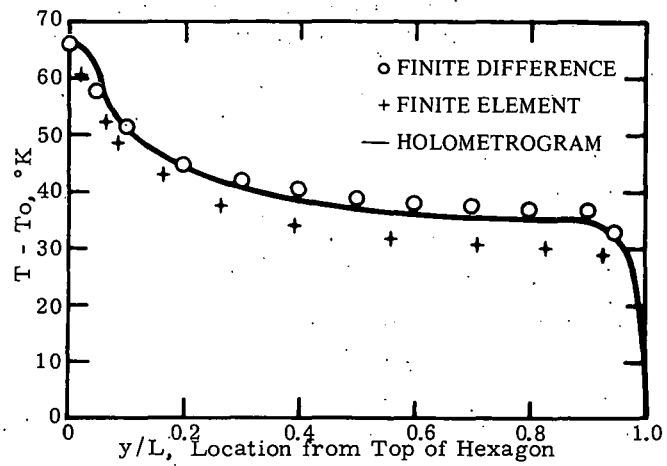

Figure 24. Measured and Predicted Temperature Profile in Test Section 2

Conclusions

The two computational methods for the general class of problems of enclosed thermally driven convection yield similar qualitative and quantitative results. Results from both methods compare favorably with the measurements of the temperature field made with a laser holographic interferometer. This optical measurement technique is shown to be a very powerful tool, yielding simultaneous temperature information over the entire flow field.

The finite-difference method is computationally more efficient than the finite-element method; nevertheless, the latter is capable of handling completely arbitrary two-dimensional geometries. The favorable comparisons shown herein lend confidence to the ability of the computational methods to produce physically realistic results for various configurations where experimental data are not available.

References

1. P. J. Roache, Computational Fluid Dynamics (Hermosa Publishers, Albuquerque, NM, 1972).

2. P. J. Roache, "Recent Developments and Problem Areas in Computational Fluid Dynamics," Lecture Notes in Mathematics, Computational Mechanics, V. 461, Springer-Verlag, Berlin (1975), p. 295.

3. J. W. Elder, "Laminar Free Convection in a Vertical Slot," J. Fluid Mech. 23 (1965), p. 77.

4. S. Ostrach, "Natural Convection in Enclosures," Adv. Heat Transfer 8, 161 (1972).

5. J. D. Hellums and S. W. Churchill, "Computation of Natural Convection by Finite-Difference Methods," ASME, Int. Developments in Heat Transfer 5 (1961), p. 984.

6. J. O. Wilkes and S. W. Churchill, "The Finite-Difference Computation of Natural Convection in a Rectangular Enclosure," AIChe Journal 12 (1966), p. 161.

7. K. Aziz and J. D. Hellums, "Numerical Solution of the Three-Dimensional Equations of Motion for Laminar Natural Convection," Phys. Fluids, 10 (1967), p. 314.

8. G. De Vahl Davis, "Laminar Natural Convection in Enclosed Rectangular Cavity," Int. J. Heat Mass Transfer 11 (1968), p. 1675.

9. A Rubel and F. Landis, "Numerical Study of Natural Convection in a Vertical Rectangular Enclosure," Phys. Fluids Suppl. 12, II (1969), p. 208.

10. K. E. Torrance, "Comparison of Finite Difference Computations of Natural Convection," J. Res. Natl. Bur. of Standards, 72B (1968), p. 281.

11. M. E. Newell and F. W. Schmidt, "Heat Transfer by Laminar Natural Convection Within Rectangular Enclosures," J. Heat Transfer, Trans. ASME, C92, 1959 (1970).

12. D. W. Larson and R. Viskanta, "Transient Combined Laminar Free Convection and Radiation in a Rectangular Enclosure," J. Fluid Mechs. 78 (1976), p. 66.

13. D. K. Gartling, "Recent Developments in the Use of Finite Element Methods in Fluid Dynamics," Computing in Applied Mechanics, AMD-Vol. 18, ASME Winter Annual, New York (1976), p. 65.

14. O. C. Zienkiewicz, The Finite Element Method in Engineering Science (McGraw-Hill, New York, 1971).

15. J. T. Oden, Finite Elements of Non-Linear Continua (McGraw-Hill, New York, 1972).

16. K. H. Huebner, The Finite Element Method for Engineers, (John Wiley and Sons, New York, 1975).

17. B. Atkinson, C. C. Card, and B. Irons, "Applications of the Finite Element Method to Creeping Flow Problems," Trans. of the Inst. Chemical Engrs., 48 (1970), p. T276.

18. P. Tong and Y. C. Fung, "Slow Particulate Viscous Flow in Channels and Tubes - Application to Biomechanics," J. Appl. Mechs., Series E, ASME, 38 (1971), p. 721.

19. E. G. Thomspon, L. R. Mack, and F. S. Lin, "Finite Element Method for Incompressible Slow Viscous Flow With a Free Surface," Developments in Mechs., 5 (Iowa State University Press, 1969), p. 93.

20. A. J. Baker, "Finite Element Solution Algorithm for Viscous Incompressible Fluid Dynamics," Int. J. for Numerical Methods in Engrng, 6 (1973), p. 89.

21. R. T. Cheng, "Numerical Solution of the Navier-Stokes Equation by the Finite Element Method," Physics of Fluids, 15 (1972), p. 2098.

22. S. L. Smith and C. A. Brebbia, "Finite Element Solution of Navier-Stokes Equation for Transient Two-Dimensional Incompressible Flow," J. of Computational Physics, 17 (1975), p. 235.

23. J. T. Oden and L. C. Wellford, "Analysis of Flow of Viscous Fluids by the Finite Element Method," AIAA Journal, 10 (1972), p. 1590.

24. D. K. Gartling and E. B. Becker, "Finite Element Analysis of Viscous Incompressible Fluid Flow, Part 1: Basic Methodology," Computer Methods in Appl. Mechs. and Engrng., 8 (1976), p. 51.

25. M. B. Hsu and R. E. Nickell, "Coupled Convective and Conductive Heat Transfer by Finite Element Methods," Finite Element Methods in Flow Problems (University of Alabama, Huntsville Press, Huntsville, AL (1974), p. 427.

26. A. O. Tay and G. DeVahl Davis, "Application of the Finite Element Method to Convection Heat Transfer Between Parallel Plates," Int. J. Heat Mass Transfer, 14 (1971), p. 1057.

27. D. K. Gartling, Finite Element Analysis of Problems in Convective Heat Transfer, SAND75-0571, Sandia Laboratories, Albuquerque, NM (1976).

28. E. Skiba, T. E. Unny, and D. S. Weaver, "A Finite Element Solution for a Class of Two-Dimensional Viscous Fluid Flow Dynamics Problems," Proceeding of the Symposium of the University of Waterloo, University of Waterloo (1971), p. 493.

29. K. W. Bedford and J. A. Liggett, "Convective Transport Finite Element Analog," J. of Engrg Mechs., ASCE, EM6, Vol. 101 (1975), p. 803.

30. D. L. Young, J. A. Liggett, and R. H. Gallagher, "Steady Stratified Circulation in a Cavity," J. of Engrg Mechs, ASCE, EM1, Vol. 102 (1976), p. 1.

31. H. W. Liepmann and A. Roshko, Elements of Gas Dynamics (John Wiley and Sons, New York, 1957).

32. R. Landenburg and D. Bershader, Physical Measurements in Gas Dynamics and Combustion, Vol. IX, High Speed Aerodynamics and Jet Propulsion (Princeton University Press, Princeton, NJ, 1954).

33. E. N. Leith and J. Upatneiks, J. Opt. Soc. America, 53 (1963), p. 1377.

34. M. Ross, Laser Applications (Academic Press, New York, 1971).

35. Lasers and Light, Readings from Scientific American (W. H. Freeman and Co., San Francisco, CA, 1969).

36. W. P. Schimmel, Jr., An Optical Measurements Laboratory for Determining Heat Transfer Coefficients, SAND76-0162, Sandia Laboratories, Albuquerque, NM (1976).

37. A. B. Witte and R. F. Wuerker, "Laser Holographic Interferometry Study of High-Speed Flow Fields," AIAA Paper No. 69-347 (1969).

38. R. D. Matulka and D. J. Collins, "Determination of Three-Dimensional Density Fields from Holographic Interferograms," J. Applied Physics, 42 (1971), p. 1109.

39. F. Mayinger and W. Pankin, "Holography in Heat and Mass Transfer," Paper IL-3, Proceedings of the Int. Heat Transfer Conference, Tokyo (1974).

40. E. A. Spiegel and G. Veronis, "On the Boussinesq Approximation for a Compressible Fluid," J. Astrophysics, 131 (1960), p. 442.

41. D. K. Gartling, "Texas Fluid Analysis Program - User's Manual," Texas Institute for Computational Mechanics Report 75-2 (1974).

42. I. Ergatoudis, B. M. Irons, and O. C. Zienkiewicz, "Curved Isoparametric, Quadrilateral Elements for Finite Element Analysis," Int. J. Solids Struc. 4 (1968), p. 31.

43. B. M. Irons, "A Frontal Solution Program for Finite Element Analysis," Int. J. Num. Math. Eng. 2 (1970), p. 5.

44. B. Carnahan, L. A. Luther, and J. O. Wilkes, Applied Numerical Methods (John Wiley and Sons, New York, 1969).

45. F. B. Hildebrande, Methods of Applied Mathematics (Princeton-Hall, New York, 1952).

46. G. D. Raithby, "A Critical Evaluation of Upstream Differencing Applied to Problems Involving Fluid Flow," Computer Math. in Appl. Mech. and Engr., 9 (1976), p. 75.

DISTRIBUTION:

TID-4500-R66, UC-79c (209)

U.S. Department of Energy (7)
Division of Reactor Development
Demonstration
Washington, DC 20545
Attn: E. S. Beckjord, Director
G. W. Cunningham, Deputy Director, Technology
H. Feinroth, Assistant Director, Technology
C. V. Backlund, Assistant Director, Facilities and Operations
R. A. Passman, Deputy Directory, Projects
C. E. Weber, Chief, Reactor Design and Analysis Branch (2)

U.S. Department of Energy (2)
Environmental Control Technology
Washington, DC 20545
Attn: W. A. Brobst
J. A. Sisler

U. S. Department of Energy
CRBRP Project Office
P. O. Box U
Oak Ridge, TN 37830
Attn: L. W. Caffey, Director

U.S. Department of Energy
FFTF Project Office
P. O. Box 550
Richland, WA 99352
Attn: R. L. Ferguson, Director

U.S. Nuclear Regulatory Commission (6)
Washington, DC 20555
Attn: W. F. Anderson
C. R. Chappell
W. Lahs
C. B. MacDonald
D. A. Nussbaumer
R. C. Shieh

National Transportation Safety Board
Bureau of Surface Transportation Safety
Washington, DC 20591
Attn: Henry H. Wakeland, Director
For: L. Brenner

National Highway Traffic Safety Administration
Office of Accident Investigation and
Data Analysis
NASSIF Building
400 7th Street, SW
Washington, DC 20590
Attn: W. E. Scott

MTB OHMO
Room 6518, Buzzards Point Building
2100 Second, SW
Washington, DC 20590
Attn: A. W. Grella

American Association of State Highway
and Transportation Officials
341 National Press Building
Washington, DC 20045

Department of Transportation (2)
Federal Highway Administration
Bureau of Motor Carrier Safety
DOT Building, Room 3406
400 7th Street, SW
Washington, DC 20590
Attn: Robert A. Kaye, Director
For: R. E. Kidwell
C. Wexler

Battelle Pacific Northwest Laboratories (2)
P. O. Box 999
Richland, WA 99352
Attn: L. D. Williams
R. J. Hall

Battelle Columbus Laboratories (3)
505 King Avenue
Columbus, OH 43201
Attn: S. J. Basham
E. C. Lusk
R. A. Robinson

U.S. Department of Energy (2)
Albuquerque Operations Office
P. O. Box 5400
Albuquerque, NM 87115
Attn: C. B. Quinn
J. A. Morley

Argonne National Laboratory
Breeder Reactor Evaluation Office
9700 South Cass Avenue
Argonne, IL 60439
Attn: C. E. Klotz, Manager

Union Carbide Corporation (3)
Oak Ridge National Laboratory
P.O. Box X
Oak Ridge, TN 37830
Attn: J. H. Evans
L. B. Shappert
W. E. Unger

Los Alamos Scientific Laboratory
P. O. Box 1663
Los Alamos, NM 87544
Attn: T. Butler, WX-8

DISTRIBUTION: (cont'd)

University of California (2)
Lawrence Livermore Laboratory
P. O. Box 808
Livermore, CA 94550
Attn: F. J. Tokarz, MS L-90
R. T. Langland, MS L-90

Hanford Engineering Development Laboratory (2)
P. O. Box 1970
Richland, WA 99352
Attn: C. L. Boyd, Manager, Fuel Handling
P. D. Shaw

E. I. DuPont de Nemours & Co.
Engineering Department
Louviers Building
Wilmington, DE 19898
Attn: J. Cherney

E. I. DuPont de Nemours & Co.
Savannah River Plant
Aiken, SC 29801
Attn: J. W. Langhaar

Electric Power Research Institute (2)
P. O. Box 10412
Palo Alto, CA 94304
Attn: C. Chan
R. K. Winkleblack

Monsanto Research Corporation
Mound Laboratory
P. O. Box 32
Miamisburg, OH 54342
Attn: D. Edling

Allied-General Nuclear Services
P. O. Box 847
Barnwell, SC 29812
Attn: R. W. Peterson

Atomics International (3)
P. O. Box 309
Canoga Park, CA 91304
Attn: E. Baumeister
K. Foster
T. Ricci

Westinghouse Electric Corporation
P. O. Box W
Oak Ridge, TN 37830
Attn: J. E. Rutenber

General Electric Company (3)
175 Curtner Avenue
San Jose, CA 95125
Attn: A. Gibson
C. Davis
R. H. Jones, M/C388

Bechtel Corporation
50 Beale Street
San Francisco, CA 94105
Attn: S. Golan

Stearns-Roger, Inc. (2)
P. O. Box 5888
Denver, CO 80217
Attn: W. H. Brinkman
R. Colasanti

NL Industries
Foot of West Street
Wilmington, DE 19801
Attn: C. Williams

Exxon Nuclear Co., Inc.
777 106th Avenue, N.E.
Bellevue, WA 98004
Attn: G. R. Waymire

The Boeing Company
P. O. Box 3707, MS 8A-68
Seattle, WA 98124
Attn: J. W. Baxter

Transnuclear, Inc. (3)
One North Broadway
White Plains, NY 10601
Attn: L. Macklin
K. Goldman
M. Rudd

J. L. Ridihalgh, President
Ridihalgh & Associates
2112 Iuka Avenue
Columbus, OH 43201

R. E. Best
Nuclear Assurance Corp.
24 Executive Park West
Atlanta, GA 30329

1000 G. A. Fowler
1200 L. D. Smith
1260 K. J. Touryan
1261 D. F. McVey
1261 D. K. Gartling (10)
1261 W. P. Schimmel, Jr. (10)
1262 H. C. Hardee
1262 C. E. Hickox
1262 D. W. Larson (10)
1280 T. B. Lane
1281 S. W. Key
1282 T. G. Priddy
1284 R. T. Othmer
1333 S. Mcalees, Jr.
2613 L. A. Bertram
5162 L. D. Bertholf

DISTRIBUTION: (cont'd)

5166 A. J. Chabai
5216 R. A. Hill
5310 W. D. Weart
5334 R. D. Klett
5400 A. W. Snyder
5410 D. J. McCloskey
5411 D. A. Dahlgren
5412 J. F. Muir
5422 R. L. Coats
Attn: H. G. Plein
5430 R. M. Jefferson
5433 R. B. Pope (20)
5433 J. M. Freedman (10)
5433 G. C. Allen, Jr. (5)
5730 H. M. Stoller
5731 R. K. Traeger
5731 J. L. Colp
8124 A. F. Baker
9337 N. R. Keltner
8266 E. A. Aas
3141 C. A. Pepmueller (Actg) (5)
3151 W. L. Garner (3)
For: DOE/TIC (Unlimited Release)